Review

Spectroscopic studies of synthetic and natural saponites: A review

Concepcion Ponce[1] and J. Theo Kloprogge[1,2*]
[1] Department of Chemistry, College of Arts and Sciences, University of the Philippines, Miag-ao, Iloilo, Philippines
[2] School of Earth and Environmental Sciences, The University of Queensland, Brisbane, Queensland 4072, Australia
* Correspondence: j.kloprogge@uq.edu.au

Abstract: Saponite is a trioctahedral 2:1 smectite with the ideal composition $M_xMg_3Al_xSi_{4-x}O_{10}(OH,F)_2.nH_2O$ (M = interlayer cation). Both the success of the saponite synthesis and the determination of its applications depends on robust knowledge of the structure and composition of saponite. Among the routine characterization techniques spectroscopic methods are the most common. This review, thus, provides an overview of various spectroscopic methods to characterize natural and synthetic saponite with focus on the extensive work by one of the authors (JTK). The IR and Raman spectra of natural and synthetic saponites are discussed in detail including the assignment of the observed bands. The crystallization of saponite is discussed based on the changes in the IR and Raman spectra and a possible crystallization model is provided. Infrared emission spectroscopy has been used to study the thermal changes of saponite in-situ including the dehydration and (partial) dehydroxylation up to 750˚C. ^{27}Al and ^{29}Si Magic-Angle-Spinning Nuclear Magnetic Resonance Spectroscopy is discussed (as well as ^{11}B and ^{71}Ga for B- and Ga-Si substitution) with respect to, in particular, Al(IV)/Al(VI) and Si/Al(IV) ratios. X-ray Photoelectron Spectroscopy provides besides chemical information also some information related to the local environments of the different elements in the saponite structure as reflected by their binding energies.

Keywords: Infrared spectroscopy; Magic-Angle-Spinning Nuclear Magnetic Resonance Spectroscopy; Raman spectroscopy; saponite, synthesis; X-ray Photoelectron Spectroscopy

1. Introduction

Clay minerals can be found as colloidal particles in sediments and soils. They comprise mainly of hydrated phyllosilicates, occasionally with variable amounts of aluminum, iron, magnesium, titanium, alkali metals, alkaline earths, and other cations. They are readily available as they comprise a substantial portion of the Earth's crust. Their importance dates to prehistoric times as seen in ancient potteries and muddy huts. Modern applications include the fields of construction engineering, petroleum exploration, recovery and refining, process chemistry and engineering, pharmaceuticals, agriculture, arts, among others. As the eventual applications of clays are determined by their structure, composition and sizes – the characterization of these properties are of utmost importance.

Among the clay minerals of interest is saponite, which has applications as: adsorbent for the removal of heavy metal ions [1,2] and carcinogenic compounds [3]; control agent of the aggregation of luminescent dyes [4,5]; matrix for controlled release of drugs [6]; catalysts for industrially important reactions [7-9] and for prebiotic chemistry [10,11] ; immobilization support for various catalysts [12-15] and many more. These applications would be dependent on properties such as size, cation-exchange capacity, plasticity, catalytic activity, swelling behavior, permeability, and substitutions in the saponite structure.

Saponite is a trioctahedral 2:1 smectite with the ideal composition $M_xMg_3Al_xSi_{4-x}O_{10}(OH,F)_2$, where M signifies the interlayer cation, e.g., Na^+, K^+, Rb^+, NH_4^+, or $1/2Ca^{2+}$, $1/2Ba^{2+}$, $l/2Mg^{2+}$, or even $1/3A1^{3+}$; and where x can range between approximately 0.3 and 0.6. A single 2:1 layer normally consists of a central sheet of octahedrally coordinated Mg^{2+} sandwiched between two sheets of tetrahedrally coordinated Si^{4+} (Figure 1). The partial substitution of Si^{4+} by $A1^{3+}$ results in an overall negative charge on the tetrahedral sheets, which is compensated by exchangeable interlayer cations. Substitution of $A1^{3+}$ can as well occur at octahedral and interlayer sites, resulting in a lower overall layer charge. Saponite got its name from Latin, sap, and Greek, sapoun, both meaning soap, alluding to its greasy or soapy feel and appearance. Saponite was first described in 1840 from Lizard Point, Landewednack, Cornwall, England. Saponite occurs as soft, massive, and plastic masses, and can be found in hydrothermal veins; basalt vesicles; and fissures cutting calc-silicates, iron-rich skarns, amphibolites and serpentinites.

A number of different saponite synthesis methods with adjustable composition and physicochemical properties have been described over the decades. These methods can be divided into sol-gel methods under mild temperatures and pressures [16-20]; hydrothermal methods which are carried out at relatively higher temperatures and pressures [8,21-26]; and microwave-assisted hydrothermal synthesis [15,27-31], which permits the crystallization to take place at lower temperatures than typical for hydrothermal processes and with strongly reduced synthesis times. The hydrothermal methods are the most commonly used synthesis methods to form saponite. Kloprogge and his co-researchers published a number of papers on the hydrothermal synthesis methods [24-26,32] and their results indicate that these techniques can be successfully applied to obtain phase pure saponite. This is seen as a result of the high hydrolysis rates of the octahedral cations precursors at high temperature and increased pressure, which support nucleation and both lateral growth and stacking of the layers of the saponite crystals. Hydrothermal methods generally involve a starting gel consisting of a stoichiometric mixture of silica, Al and Mg salts and a source of interlayer cations (typically sodium or ammonium, but other cations have also been reported, see e.g [24]) which is allowed to react under hydrothermal conditions at temperatures between 150 and 450 ˚C under autogenous water vapor pressures for variable time periods from as short as 5 min up to 3 months.

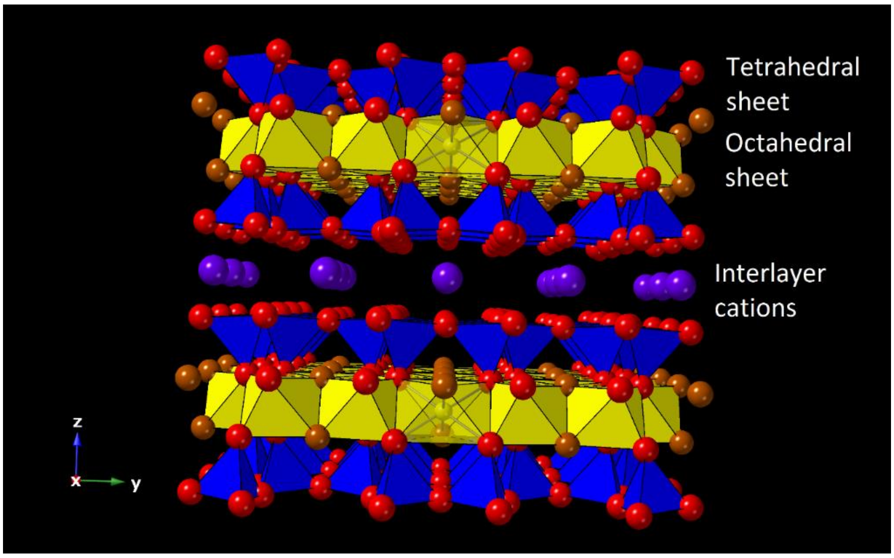

Figure 1. Ideal structure of saponites showing the tetrahedral (Si, Al) and octahedral (Mg) sheets and interlayer space with interlayer cations (Na, K, Ca, etc.).

The mild non-hydrothermal saponite synthesis method using urea described by Vogels *et al*. is worth noting [18]. It presents a simple method to prepare large volumes of saponites with extensive control on the texture in addition to the composition, though the crystallinity was generally lower compared to hydrothermally formed saponite. The saponites were synthesized at a constant mild temperature of 90 °C. The starting Si/Al gel was prepared using a simple procedure of diluting Na_2SiO_3 solution in demineralized water and slowly adding under continuous stirring $Al(OH)_4^-$ to form the gel. The gels were then added to demineralized water and heated to 90 °C. The required

doi:10.20944/preprints202011.0312.v1

masses of nitrates of the divalent octahedral M^{2+} cations ($M^{2+} = Mg^{2+}$, Ni^{2+}, Zn^{2+}, Co^{2+}, and Cu^{2+}) and urea were dissolved in water and afterwards added to the gel-water mixture (maintained at 90 °C) after which the synthesis started.

The success of the saponite synthesis process and the determination of its applications depends on robust knowledge of the various characterization techniques of the structure and composition of saponite. Among the routine characterization techniques for the composition-structure-properties relationship in saponite, spectroscopy is the most common. This review, thus, provides an overview of various spectroscopic methods to characterize natural and synthetic saponite with focus on the extensive work performed by Kloprogge and co-workers in various research groups over the past 25-30 years. Infrared (IR) spectroscopy is clearly the most important and common spectroscopic technique to investigate saponite. Raman spectroscopy can also provide valuable information about the low-wavenumber region of saponite, which is difficult to obtain with IR spectroscopy (Far-IR region below 400 cm^{-1}). The information obtained from mid-IR (MIR) spectroscopy is not the same as that from Raman spectroscopy, as the physics involved in Raman spectroscopy are very different from those of IR spectroscopy and these two techniques are often used in complement to each other. Solid-state magic-angle-spinning nuclear magnetic resonance (MAS-NMR) spectroscopy is a method that use magnetic properties of certain elements, here in particular ^{27}Al and ^{29}Si, to obtain detailed information concerning the local environment of Si and Al in the tetrahedral and octahedral sheets of the saponite structure (coordination, influence of nearest and next-nearest neighbor atoms), though other elements have also been studied (see e.g. ^{23}Na NMR of synthetic beidellite, a smectite closely related to saponite [33]). For clay minerals this includes especially the local environments of Si and Al in the tetrahedral and octahedral sheets. Finally, the application of X-ray photoelectron spectroscopy (XPS) to study saponite, is reviewed.

2. Materials and Methods

The materials and methods described in this section are from the works of Kloprogge and co-researchers in various research laboratories over the past 25-30 years.

2.1. Hydrothermal synthesis

Kloprogge and co-workers synthesized ammonium saponite by preparing a homogeneous powder mixture of amorphous silica (SiO_2), aluminum triisopropylate ($AI[OCH(CH_3)_2]_3$), and magnesium acetate-tetrahydrate ($[CH_3COO]_2Mg{\cdot}4H_2O$) mixed with aqueous ammonium hydroxide solution [25]. When different interlayer cations such as Na^+, K^+, Rb^+, Ca^{2+}, Ba^{2+}, or Ce^{4+} are desired, the homogenous powder is mixed with a solution comprising the preferred cation in the form of a hydroxide or fluoride salt. The subsequent stoichiometric gel had the theoretical saponite formula $M_{0.6}Mg_3Al_{0.6}Si_{3.4}O_{10}(OH)_2$, where M signifies the interlayer cation [24,25]. Approximately 125 g of the above gel was hydrothermally treated for 72 hr at 200 °C under autogenous water pressure. Kloprogge et al. [24] have shown that a crystalline yield near 100% is possible under these conditions. The resulting crystalline saponites were cooled, separated from the coexisting hydrothermal fluid, washed twice with distilled water to remove possible free salts, centrifuged, and dried overnight at 120 ˚C. The suite of ammonium-saponites discussed in this review was synthesized and extensively characterized by Kloprogge and co-workers [24,25,34].

2.2. Urea assisted synthesis

A Si/Al gel with a Si/Al molar ratio of 5.67 (x = 1.2) was prepared by diluting 40 g of a Na_2SiO_3 solution (27 wt% SiO_2) in 100 mL demineralized water. This Si-containing solution was slowly mixed to a previously prepared $Al(OH)_4^-$ made by dissolving 11.9 g $Al(NO_3)_3{\cdot}9H_2O$ in a 80 mL 2 M NaOH solution. This mixing turned an initially clear solution cloudy with subsequent formation into a gel. When the gel formed, stirring was stopped and the mixture was allowed to stand for one hour prior to further use. The gels formed from this process did not contain excess liquid and were not further treated. Gels with different Si/Al molar ratios were prepared in a similar way by altering the amounts of aluminum nitrate and sodium silicate. The total amount of Si + Al was kept constant. A gel with a

Si/Al ratio of 39.0 (x = 0.2) was prepared in a somewhat different way, since after mixing the Si- and Al-containing solutions no gelation occurred. After addition of 10 mL HNO_3 (65%), though, a stable white gel was formed. Gels with an extremely low Si/Al ratio of 2.33 (x = 2.4) were prepared similar to the other Si/Al gels, but without NaOH addition in the Al-containing solutions. This had to be done to reduce the rate of gelation. 1000 mL of demineralized water was added to the final gel and heated to 90 °C. For Ga-containing saponites, instead of $Al(OH)_4^-$, $Ga(OH)_4^-$ was used. The $Ga(OH)_4^-$ solution was prepared from a strongly dilute 8M $GaCl_3$ stock solution in a NaOH solution. B-containing saponites were synthesized following two different methods: the "aerosol" and the "gel" method described above. The Aerosil method involved mixing approximately 10g aerosil (380V, Degussa) and an amount of borax ($Na_2B_4O_7$) corresponding to a Si/B molar ratio of 2.9–12.3 in 1500ml demineralized water.

The required amounts of $Mg(NO_3)_2{\cdot}6H_2O$, $Ni(NO_3)_2{\cdot}6H_2O$, $Zn(NO_3)_2{\cdot}4H_2O$, $Co(NO_3)_2{\cdot}6H_2O$, and/or $Cu(NO_3)_2{\cdot}3H_2O$, and typically 36.0 g urea, were dissolved in 500 mL water and added to the gel-water mixture (maintained at 90 °C) after which the synthesis started. Addition of the above solution resulted in a slight temperature drop of the synthesis mixture by about 10 °C. No acidification of the synthesis mixture was performed before the start of the synthesis procedure since the gels were not stable in acidified solutions. Saponites with octahedral sheets consisting of two metals were prepared by using the required combination of the divalent metal nitrate salts, with the ratio between the cations varied between 1 to 29, in the synthesis mixture. A set of experiments for the Zn-saponite preparation was also carried out with variable amounts of urea to investigate the effect of the concentration of the hydrolyzing urea on saponite formation. The amounts of urea in the starting mixture were 0.0, 18.0, and 72.1 g. An additional synthesis was performed using 36.0 g urea together with additional NaOH, which raised the pH to a level of 8 in the initial mixture. The synthesis duration was kept constant at 20 hours unless otherwise indicated. After the desired period of time of synthesis, the cloudy suspensions were filtered. The white (Zn, Mg), light-green (Ni), pink (Co), or light-blue (Cu) filtrates were washed thoroughly with demineralized water and dried overnight at 130 °C before characterization. The suite of saponites discussed in this review was extensively characterized by Vogels and co-workers [18,35-37].

2.3. Natural saponites

Four different natural saponites were used in this study: SapCa-1 and SapCa-2 (Clay Minerals Society source clay, Ballerat, Ca, contains less than 3 % diopside), 1433 (Ruduo, Poland, sample from the collection of Prof. van der Marel, courtesy Sjerry van der Gaast, NIOZ The Netherlands) and Ca-saturated saponite from Milford, Utah (sample from CSIRO Adelaide, Australia, courtesy Phil Slate). X-ray diffraction was used to verify the trioctahedral saponitic nature of the natural samples and ascertain the absence of major impurities.

2.4. Spectroscopic methods

2.4.1. Mid-infrared spectroscopy

All saponites were oven-dried to remove any adsorbed water and stored in a desiccator. For each sample 1 mg. was finely mixed with 250 mg of oven-dried spectroscopic grade KBr having a refractive index of 1.559 and a particle size of 5–20 mm and pressed into a disc using 8 ton of pressure for 5 min under vacuum. Kloprogge and co-workers used a Perkin-Elmer 1600 series FT-IR spectrometer to record in triplicate the spectrum of each sample. The settings used were 64 scans at 4 cm^{-1} resolution between 400 and 4000 cm^{-1}.

2.4.2. Raman spectroscopy

The FT-Raman spectroscopic analyses were performed on a Perkin-Elmer System 2000 FT spectrometer equipped with a Raman accessory comprising a Spectron Laser Systems SL301 Nd:YAG laser operating a wavelength of 1064 nm. For the natural saponites, 275 scans were obtained at a spectral resolution of 4 cm^{-1} between 200 and 4000 cm^{-1}, whereas for the synthetic samples, 1000 scans were necessary in order to obtain an acceptable signal/noise ratio.

2.4.3. Infrared emission spectroscopy (IES)

Infrared emission spectroscopy is becoming an important technique for measuring discrete vibrational frequencies emitted by thermally excited molecules. The IES measurements featured in this review were performed on a Digilab FTS-60A spectrometer modified by replacing the original IR source with an emission cell. For a detailed description of the cell and the principles of the experiment, the reader is directed to [38]. In this technique, the sample preparation involved spreading as a thin layer about 0.2 mg of the clay saponite on a 6 mm diameter platinum surface while keeping an inert atmosphere within a nitrogen-purged cell during heating. The platinum disk served as a hot plate to heat the sample and is placed on the graphite rod. The infrared emission cell is composed of a modified atomic absorption graphite rod furnace driven by a thyristor-controlled AC power supply capable of delivering up to 150 amps at 12 volts. The thermocouple junction is held at less than 0.2 mm below the surface of the platinum by an insulated 125-µm type R thermocouple embedded inside the platinum plate. A Eurotherm Model 808 proportional temperature controller, coupled to the thermocouple, keeps the temperature at ± 2 °C of the operating temperature of the saponite sample. The layout of the IES facility is based on an off axis paraboloidal mirror with a focal length of 25 mm mounted above the heater capturing the emitted infrared radiation and directing this radiation into the spectrometer. The assembly of the heating block, and platinum hot plate is located such that the surface of the platinum is slightly above the focal point of the off axis paraboloidal mirror. In that way the geometry is such that a roughly 3 mm diameter area is sampled by the spectrometer. The original spectrometer was adapted for IES by the removal of the original source assembly and mounting a gold-coated mirror, which was drilled through the center to allow the passage of the laser beam. The mirror was mounted at a 45° angle, so that the IR radiation is directed into the FTIR spectrometer. In a normal set of experiments, 3 sets of spectra are collected: 1) the black body radiation over the temperature range selected at the various temperatures, 2) the platinum plate radiation is collected at the same temperatures and 3) the spectra from the Pt plate covered with the sample also at the same temperatures. Normally a single set of black body and Pt radiation is required per day. The emittance spectrum at a particular temperature can be calculated by first subtracting the single beam spectrum of the Pt backplate from that of the Pt + sample, and secondly the resulting difference spectrum is ratioed to the single beam spectrum of the approximate blackbody (graphite). This spectral manipulation is performed after all the spectra have been collected. The emission spectra were collected at intervals of 50 °C over the temperature range from 200 to 750 °C. The time between scans (while the temperature was raised to the next hold point) was ±100 seconds. It was considered that this was sufficient time for the heating block and the powdered sample to reach temperature equilibrium. The spectra were acquired by coaddition of 64 scans for the whole temperature range (approximate scanning time 45 seconds), with a nominal resolution of 4 cm^{-1} in the range between 4000 and 400 cm^{-1}. Good quality spectra can be obtained provided the sample thickness is not too large. If too large (i.e. too thick a layer) a sample is used, then the spectra become difficult to interpret because of effects related to self-absorption.

2.4.4. Spectral manipulation

Spectral manipulation for Mid-infrared, Raman and IES, such as baseline adjustment, smoothing and normalization was performed using the Spectracalc software package (Galactic Industries Corporation, NH, USA).

2.4.5 Magic-Angle-Spinning Nuclear Magnetic Resonance Spectroscopy (MAS-NMR)

The synthetic NH_4-saponites were analyzed by MAS-NMR by Kloprogge *et al.* [39] at Shell Research Laboratory in Amsterdam, The Netherlands. ^{29}Si solid-state MAS-NMR spectra of the hydrothermal saponites were recorded at 59.62 MHz on a Bruker CXP-300 spectrometer (magnetic field 7.05 T). $^{27}A1$ solid-state MAS-NMR spectra of the hydrothermal saponites were obtained on a Bruker WM-500 spectrometer (130.32 MHz, magnetic field 11.7 T). Both instruments apply a sample spinning rate of approximately 14 kHz. Approximately 4500 Free Induction Decays (FIDs) were accumulated at a repetition time of 12 s (pulse width 3.25 µs) for the ^{29}Si spectra and 3000 FIDs were accumulated at a repetition time of 0.8 s (pulse width 3.0 µs) for the $^{27}A1$ spectra. Chemical shifts are given in ppm relative to tetramethylsilane (TMS) and $[Al(H_2O)_6]^{3+}$ respectively. Upfield shifts are taken to be negative. Since the spectra were recorded with a shielded aluminum-free probe, no correction was needed for background signals. Deconvolution of the spectra was obtained by fitting the signals to independent Gaussian lines using a least-squares method.

Vogels *et al.* [18] performed high-resolution solid-state MAS-NMR measurements on the urea synthesized saponites with a Bruker AM-500 spectrometer (117 T) at the SON HF-NMR facility, University of Nijmegen, Nijmegen, The Netherlands. ^{27}Al MAS-NMR experiments were done at 130.321 MHz with a pulse length of l μs and a pulse interval of 1 second. ^{29}Si MAS-NMR experiments were run at 99.364 MHz with a pulse length of 6.5 μs and a pulse interval of 40s. Chemical shifts (δ) of ^{27}Al and 29Si are reported in ppm relative to $[Al(H_2O)_6]^{3+}$ and $[(CH_3)_4Si]$ respectively.

2.4.6 X-ray Photoelectron Spectroscopy (XPS)

The clay minerals were analyzed in freshly powdered form in order to prevent surface oxidation changes. Prior to the analysis the samples were outgassed under vacuum for 72 h. The XPS analyses were performed on a Kratos AXIS Ultra with a monochromatic Al X-ray source at 150 W under ultrahigh vacuum conditions (10^{-9} to 10^{-10} Torr). Each analysis started with a survey scan from 0 to 1200 eV with a dwell time of 100 ms, pass energy of 160 eV at steps of 1 eV with 1 sweep. For the high resolution analyses the number of sweeps was increased, the pass energy was lowered to 20 eV at steps of 100 meV and the dwell time was changed to 250 ms. In order to account for the possibility of heterogeneity in the clay samples three different analyses were obtained for each clay sample. The Kratos Axis Ultra, XPS used for the analysis, has a built-in patented coaxial low energy electron charge compensation system which provides a high flux of electrons of uniform charge density. It uses a magnetic immersion lens situated below the sample and, the low energy electrons from a filament located at the base of the photoelectron input lens, are injected into the magnetic field. It is operated in such a way that ‘overcompensation’ occurs which results in full charge neutralization and the photoelectron peaks move down scale a few eV. The spectra were charge corrected using the advantageous C 1s signal at 285 eV. Band component analysis was undertaken using the Jandel ‘Peakfit’ software package, which enabled the type of fitting function to be selected and allows specific parameters to be fixed or varied accordingly. Band fitting was done using a Lorentz–Gauss cross-product function with the minimum number of component bands used for the fitting process. The Gaussian–Lorentzian ratio was maintained at values greater than 0.7 and fitting was undertaken until reproducible results were obtained with correlations of r2 greater than 0.995.

3. Mid-infrared and Raman spectroscopy

3.1 General characterization of the IR and Raman spectra of saponite

Generally, octahedrally coordinated Mg dominates in natural saponite; a partial substitution of Al^{3+} for Si^{4+} substitutions in the tetrahedral sheets, in addition to some Al^3, Fe^{2+} or F^{3+} + for Mg^{2+} substitution in the octahedral sheet is frequently observed. Partly due to these tetrahedral and octahedral substitutions, the Mid-IR spectra of both natural and synthetic saponites exhibit significant difference to that of talc, $Mg_3Si_4O_{10}(OH)_2$; i.e., the bands are broader and slightly shifted (Figure 2). The OH stretching region of saponite (Ballarat, California) shows characteristically weak ν(Mg_3-OH) band near 3680 cm^{-1} with a weak band near 3720 cm^{-1}. When a KBr pellet containing saponite is heated (to eliminate adsorbed H_2O), the highly localised negative charge on the interlayer surface of the tetrahedral sheet attracts the K^+ ions from the KBr, which affects the orientation of the OH groups, and a high-wavenumber ν(Mg_3-OH) satellite appears [40,41]. The main Si-O stretching vibration of saponite is found at 1006 cm^{-1}, slightly lower than for hectorite due to Al for Si substitution in the tetrahedral sheet (Figure 3). Likewise, as for talc, the bands at 691 and 661 cm^{-1} for saponite, consist of the contributions of the perpendicular Si-O and bending Mg_3-OH vibrations. These bands show broadening similar to the dioctahedral smectites (with trivalent metals in the octahedral sheet) caused by local disorder. The band around 530 cm^{-1} belongs to the perpendicular Mg-O vibrational mode. Finally, the spectra of saponites exhibit two bands at 460 and 443 cm^{-1} assigned to the OH-translation and Si-O-Si bending vibrational modes, respectively (Table 1).

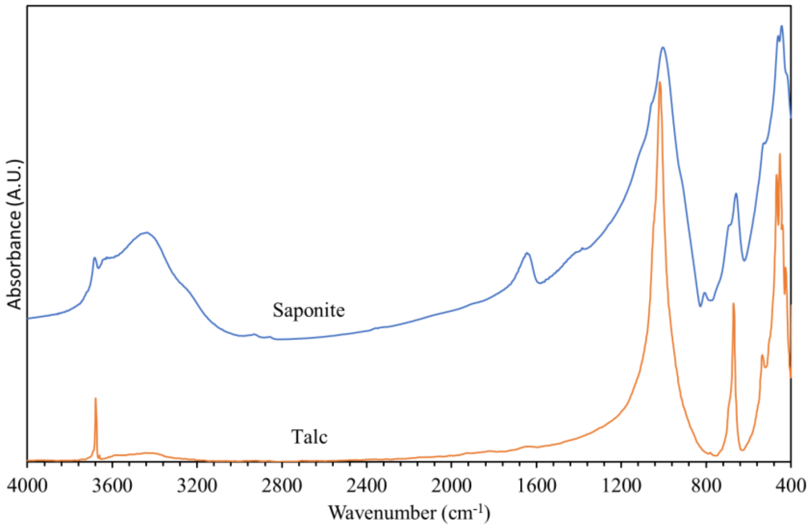

Figure 2. IR ATR spectra of saponite (Ballarat, California) and synthetic talc showing the broader and slightly shifted bands for saponite in comparison to talc.

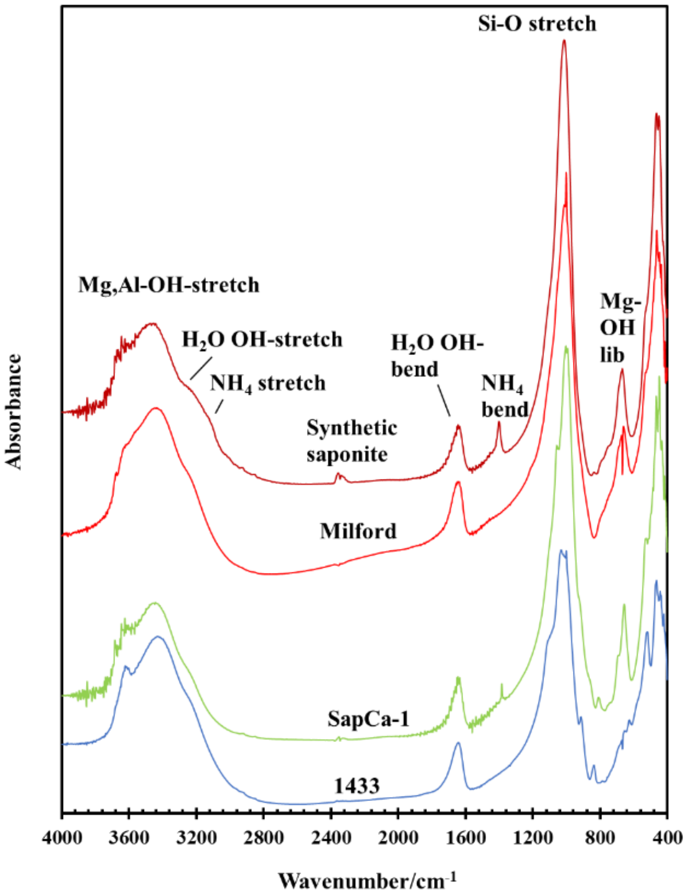

Figure 3. Mid-IR absorption spectra of 3 natural (1433, SapCa-1, Milford) and 1 synthetic NH_4-saponite

For smectites the OH-stretching region in the MIR spectra exhibits not only the bands associated with the hydroxyl groups of the octahedral sheets but also by physisorbed and interlayer water. In the equivalent Raman spectra the effect of physisorbed and interlayer water is far more challenging to detect. Obtaining Raman spectra of smectites is usually complicated by the occurance of strong fluorescence, and consequently meticulous experimentation is necessary to acquire useful spectra. The main Raman bands for saponite occur around 3680 and 3420 cm^{-1} [42,43]. The sharp intense band around 3680 cm^{-1} has been assigned to the ν(Mg_3-OH) vibrational mode, similar to the IR band at this position, and the broad band around 3420 cm^{-1} to the ν(H_2O) vibrational mode of interlayer water. To gain a better understanding of the changes of octahedral ν(M_3^{2+}-OH) modes (M^{2+} here is a divalent atom in the octahedral sheet, in saponite mainly Mg^{2+}) as affected by increasing tetrahedral layer charge, IR and Raman spectra were obtained of a number of synthetic saponites by Pelletier *et al.* [44]. With increasing layer charge, the IR and Raman spectra both exhibited a continuous shift of the ν($M^{2+}{}_3$-OH) from about 3678 to about 3686 cm^{-1}. In the IR and Raman spectra of K-saponites two principal bands were found at 3683 and 3720 cm^{-1}. With increasing layer charge, the intensity of the latter band increased, and the relative integrated intensity was basically proportionate to the layer charge, suggesting interlayer K^+ was positioned near the isomorphic substitution sites in the tetrahedral sheet and affected the structural hydroxyl groups. In addition, this demonstrates that the structural hydroxyl groups may form hydrogen-bonds across the ditrigonal cavity where the isomorphic tetrahedral substitutions are located. The band at about 3720 cm^{-1} has been attributed to structural OH-groups affected by the existence of K^+ ions above or within the ditrigonal cavity of the tetrahedral sheet [40], whereas the ~3683 cm^{-1} band has been assigned to unperturbed hydroxyl-groups. To interpret the spectra measured for hydrated Na^+ saponites in the OH-stretching region, the Raman spectra were deconvoluted into four ν($M^{2+}{}_3$-OH) bands at about 3675, 3680, 3685 and 3690 cm^{-1}. The changes with layer charge of the relative percentages of these four bands was explained by accounting for the position of the hydrated interlayer cations associated with the distribution of the isomorphic tetrahedral substitutions. This hypothesis was verified by applying a straightforward statistical model, which produced four different types of OH groups in the octahedral sheet of hydrated Na-saponites [44].

Rinnert *et al.* [45] demonstrated that Na-saponite still had a substantial amount of interlayer water (equivalent to 1 H_2O molecule per 2 Na^+ cations) even after dehydration at 100 °C at 0.1 Pa. The Raman spectrum in the range between 3600 and 3750 cm^{-1} exhibited two broad bands at around 3675 and 3712 cm^{-1}. The band at 3675 cm^{-1} was assigned to unperturbed hydroxyl-groups, whereas the other band at 3712 cm^{-1} was attributed to hydroxyl-groups perturbed by nearby Na^+ cations, positioned near the ditrigonal cavity consistent with the analysis by Pelletier *et al.* [44]. Rinnert *et al.* [45] indicated that in the dehydrated state, every interlayer Na^+ ion perturbs up to two structural hydroxyl-bands, the band width showing the variation in relative influence of perturbation. This would, though, greatly hinge on how good individual layers are stacked. Because the isomorphic tetrahedral substitutions are random in smectites, such as saponite, the ideal fitting necessary for proper crystalline stacking is not present. For partial pressures between 0.06 and 0.18, the amount of adsorbed water increased significantly up to 4.5 mmol/g, which is equivalent to around 1.5 H_2O molecule per interlayer cation. Under these conditions, the basal spacing increased to 12.3 Å, which is historically attributed to a one-layer hydrate state (1-LHS). This proved that the change to the full 1-LHS was linked to the solvation of the interlayer Na^+ by three H_2O molecules, similar to what was determined before for hectorite by MIR spectroscopy [46].

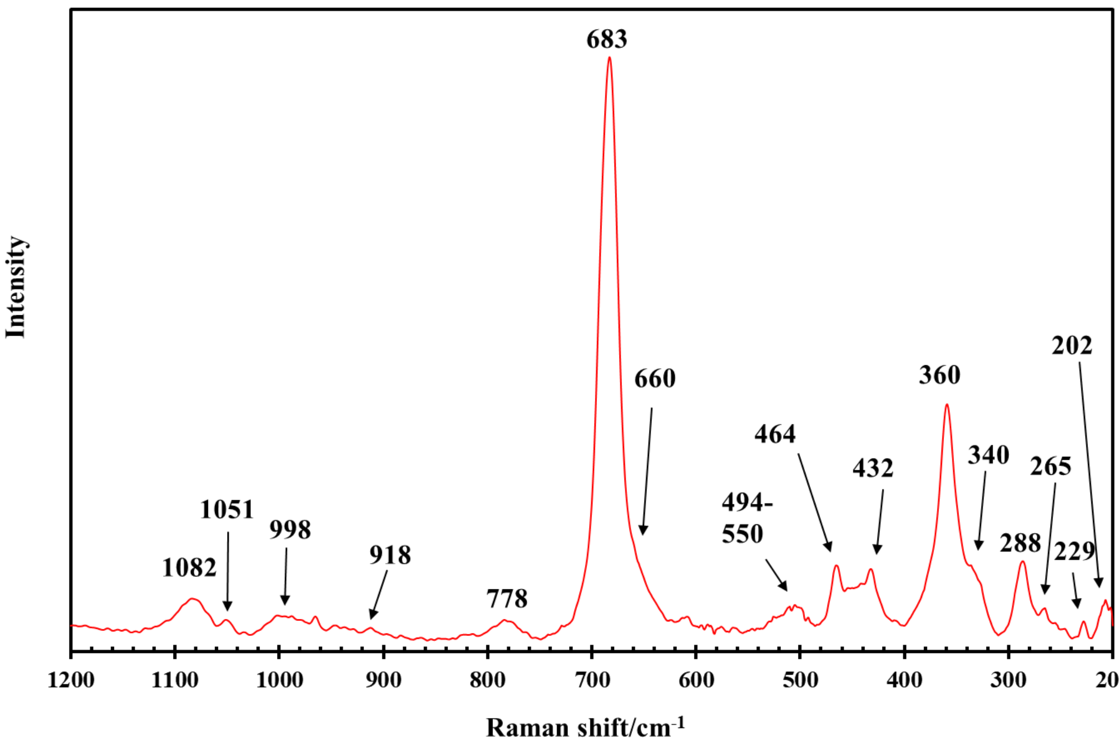

Figure 4. Raman spectrum of natural saponite (Milford) in the region between 1200 and 200 cm^{-1}.

Farmer [47] explained the pseudo-hexagonal tetrahedral sheet in layer silicates centered around the highest possible symmetry (C_{6v}) for the SiO_4 tetrahedron as a separate unit. The vibrational modes can subsequently be categorized in five species: $2A_1+3B_1+1B_2+3E_1$ and $3E_2$. Of these species just A_1 and E_1 are IR active, whereas A_1, E_1 and E_2 are in theory Raman active. Calculations suggest that the following modes 902 (a_1^1), 611 (a_1^2), 130 (b_2), 915 (b_1^1), 779 (b_1^2), 319 (b_1^3), 1015 (e_1^1), 543 (e_1^2), 285 (e_1^3), 695 (e_2^1), 499 (e_2^2) and 127 cm^{-1} (e_2^3) are likely. Nevertheless, when the SiO_4 tetrahedron is examined within the tetrahedral sheet of clay minerals a reduction in symmetry must be taken into account. Still, the C_{6v} approximation forms a logical point to stat at for understanding the lower wavenumber region in the Raman and IR spectra of smectites, such as saponite.

The Raman spectrum of saponite in the region below 1200 cm^{-1}, where Mg^{2+} cations form the octahedral cations and tetrahedral substitution Al^{3+} for Si^{4+} is typical, exhibits a relatively simple spectrum. Most of the bands are vibrational modes associated with distorted $(Si,Al)O_4$ tetrahedra. The strongest bands are the Si–O vibrational modes at 1082, 683, 464, 432 and 360 cm^{-1} (Figure 4). Furthermore, two less intense bands at 1051 and 998 cm^{-1} along with a band at 288 cm^{-1} have been attributed to the vibrational modes of the SiO_4 tetrahedra [47,48]. In the very low-wavenumber region only one vibrational mode of the distorted MgO_6 at 201–202 cm^{-1} has been detected. Wang *et al*. [42,43] described some bands for a greyish green saponite found in fine-grained weathered basalt matrix. This saponite exhibited major Raman bands around 680, 355, 295 and 190 cm^{-1} with the 190 cm^{-1} band attributed to the $\nu_1(A_{1g})$ $(Al,Mg)O_6$. It exhibited only a low intensity band in the 1000 cm^{-1} region of the Raman spectrum. A Raman band in the range between 370 and 330 cm^{-1} found for trioctahedral smectites (i.e. smectites with divalent metals in the octahedral position) has tentatively been attributed to SiO_4 bending vibrations [34]; nevertheless, the involvement of the MgO_6 unit [49] should also be taken into consideration.

Table 1 Raman and mid-IR band positions and suggested assignments for Milford and synthetic NH_4-saponite

Raman	IR	IR	Assignment [34,50,51]
Milford Saponite		NH_4-saponite	
202			$\nu_1(A_{1g})$ $(Mg,Al)O_6$
229			
265			$A_1(\nu_1)$ OH-O triangle
288			e_1^3 SiO_4
340			$\nu_2(e)$ SiO_4 or b_1^3 SiO_4
360			$\nu_5(e)$ SiO_4, MgO_6
	424	422	? SiO_4
432			$\nu_3(a_1)$ SiO_4 or e_1^2 SiO_4
	447	449	e_2^1 SiO_4
464	465	461	$\nu_6(e)$ SiO_4 (R), Mg_2Al-OH translation (IR)
494-540	528	529	e_1^2 SiO_4 (R), Mg_3-OH perpendicular (IR)
659	654	665	Mg_3-OH libration
683	696	691	$\nu_2(a_1)$ SiO_4 (R), e_2^1 SiO_4 (IR)
		740	Mg_2Al-OH deformation
776	787	779	b_1^2
	838	836	δ(AlMgOH) (R), Al-O apical AlO_4 (IR)
918		912	$\delta(Al_2OH)$, b_1^1
998	1010	1020	$\nu_1(a_1)$ SiO_4 (R), e_1^1 SiO_4 (IR)
1050			$\nu_4(e)$ SiO_4
1082	1110	1111	$\nu_3(f_2)$ SiO_4 (R), Si-O stretch (IR)
	1165		Si-O stretch
		1430	NH_4 bend
		1635	water OH-bend
		3118	NH_4 stretch
	3222	3218	water OH-stretch
	3420	3431	water OH-stretch
	3625	3589	Mg_2(Al,vac)-OH stretch
	3674	3662	Mg_3-OH stretch
		3778	Si-OH stretch

3.2. *Effect of hydrothermal synthesis temperature*

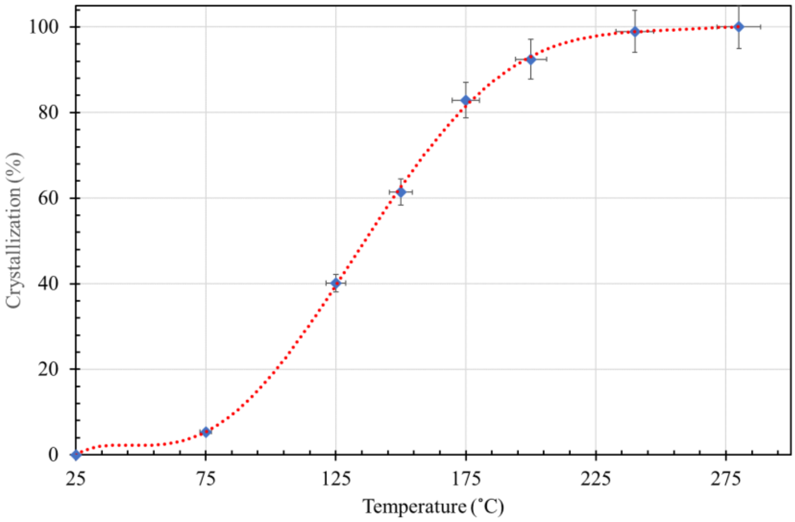

Figure 5 Percentage of saponite crystallization as function of synthesis temperature (modified after [25]).

Generally, the crystallisation of clay minerals from dilute solution is assumed to start with the formation of octahedral sheets to which, at the same time or shortly after the octahedral sheets are formed, the tetrahedral sheets are attached to form single layers (e.g. [32]). This mechanism is centered around the notion that SiO_4 tetrahedra will never freely polymerize into a twodimensional network in solution, but instead will form a threedimensional network. The formation of a two-dimensional silica tetrahedral network, as found in the tetrahedral sheets of clay minerals, hence is believed it needs some sort of template to attach to, most probable to be the initial stages of the octahedral sheet formed due to the low solubility of, for example, Al^{3+} hydroxides near neutral pH values. The results published by Kloprogge *et al.* [25] and Vogels *et al.* [26] on the synthesis of saponites, though, indicate a mechanism initiating as slow transformations within the amorphous starting gel [34,52-57]. Figure 5 shows the progress of the saponite crystallization as function of synthesis temperature under hydrothermal conditions,with the initial slow crystallization followed by a rapid increase between 75 and 200 ˚C, until all amorphous material has reacted at around 240 ˚C. Their crystallisation mechanism was centered around the low solubility of silica in the pH range found during the crystallization. The existence of amorphous silica was easily observed in the FTIR spectra with broad bands in the 1000–1250 cm^{-1} region. During crystallization, the SiO_2 configuration changed from a disordered, three-dimensional network in the amorphous state to a more ordered, maybe already a two-dimensional, structure as typically present in the tetrahedral sheets of clay minerals such as saponite,. as shown by the disappearance of the bands at 900–910 and 1225 cm^{-1} and the continuous shift to lower wavenumbers of the initial 1043 cm^{-1} band. Since two overlapping bands around 660 and 690 cm^{-1} were determind to appear almost at the same time before to the disappearance of the wide band at about 1250 cm^{-1} associated with amorphous silica, suggest that the octahedral and tetrahedral sheets in the saponite structure formed nearly at the same time. Sharpening of the other vibrations related to the various ν(SiO) modes was not found until the temperature reached about 200 °C. The presence of tetrahedral Al^{3+} substitution for Si^{4+} was only observed in saponites synthesized at 240 °C and 280 °C with the appearance of a new band at 837 cm^{-1}. The formation of the octahedral sheets with both Mg^{2+} and Al^{3+} was revealed by the presence of bands due to both Mg^{2+} and Al^{3+} still bonded to hydroxyl groups at higher temperatures. This concurs with earlier studies by Kloprogge *et al*. [24,25] and Vogels *et al.* [26] that the Al^{3+} at the beginning stayed in solution until the pH dropped to values near neutral, forcing the Al^{3+} to be built into the saponite structure at a later stage of the crystallisation.

Vogels *et al.* [18] described that octahedral divalent cation substitution shifted to IR bands towards lower wavenumbers relative to natural saponite from Krugersdorp [58]. The ν(Mg_3-OH) band at 3670 cm^{-1} for natural Mg^{2+}-saponite moved to 3632 cm^{-1} (Zn^{2+}-saponite), 3620 cm^{-1} (Co^{2+}-saponite), and finally 3616 cm^{-1} (Ni^{2+}-saponite). All these synthetic saponites showed sharp bands between 3600 and 3800 cm^{-1}. Partially or completely dehydrated natural and synthetic saponites typically exhibited two characteristic ν(M_3-OH) modes and calcination at temperatures up to 500°C did not visibly alter their positions. The position of the other ν(M_3-OH) band varies with the compensating cation [41,44] and is shifted because of electronegativity differences of these octahedral cations [59]. Synthetic Ni-saponite also showed a minor third band at about 3700 cm^{-1}, the origin of which was not clear at the time. Distinguishing between these bands is complicated when the saaponites are hydrated caused by overlap with the broad ν(H_2O) band of physisorbed and interlayer H_2O. The ν_2(OH) band in this region, associated with 'free' OH groups [41,44], was hardly observed as a separate shoulder in hydrated saponites, but after partial dehydration of the saponite the band at 3732 cm^{-1} became distinctly visible. Farmer [47] originally ascribed this band to M_3-(OH) units within the octahedral sheets influenced by the electric field related to the interlayer cations, however, Pelletier *et al*. [41,44] found the ν_2(M_3-OH) band position to be independent from the Si^{4+}/Al^{3+} ratio and the type of octahedral or interlayer cation. Consequently, this band may as an alternative come from from hydroxyl-groups coordinated to the tetrahedral sheets at the external surface of the clay particle as Si–OH (silanol). The stretching vibration of similar terminal silanol groups in zeolites has been observed at similar wavenumbers [60].

Baldermann *et al.* [61] investigated the Fe^{3+}–Mg^{2+}-saponite solid solution series and found the ν(Mg_3-OH) and ν(Mg_2Al-OH) bands to be of relatively weak intensity (3680 cm^{-1}) or even absent (3630 cm^{-1}) in the synthesised ferrous saponite. Iron substitution in Mg-rich clay minerals normally shifts the ν(Mg_3-OH) to lower wavenumbers [62] and the synthetic Fe-Mg-saponites exhibited some, but not competely resolved modulations below 3680 cm^{-1} that could be related to such substitutions. In these precipitates an intense IR band was found at about 3560 cm^{-1}, which was interpreted to belong to the dioctahedral ν($Fe^{3+}{}_2$OH) or ν(Fe^{3+}MgOH) mode [63]. Such an attribution is validated by the observation of a band at 816 cm^{-1}. Nevertheless, the δ(Mg_3-OH) band at 680 cm^{-1} present in all spectra of the Fe-Mg-saponites, distinctly suggest the dominance of trioctahedral structural units. The IR bands below 500 cm^{-1} that could help to differentiate between trioctahedral and dioctahedral structural units in the octahedral sheet were not well resolved and consequently could not be used.

The microwave assisted crystallization of saponite was described by Vicente *et al.* [31] and Trujillano *et al.* [28], where the emergence of one intense band around 1105 cm^{-1} in combination with a shoulder at 1200 cm^{-1} verified the presence of the amorphous silica phase, as also determined by XRD, which was a function of the Mg^{2+} source and the corresponding pH in the starting material. The presence of a single band at 1027 cm^{-1} attributed to the ν(SiO) ordered within layers for the saponites formed under neutral to slightly basic (7–8) conditions using $Mg(CH_3COO)_2$. Three other IR bands were found at 1401, 3675 and 666 cm^{-1}, which are due to the NH_4^+ bending, e ν(Mg_3-OH), and δ(Mg_3-OH) vibrational modes, respectively [31]. Trujillano *et al.* [28] described two shoulders at 3650 and 3630 cm^{-1} attributed to ν(Mg_3-OH), and signify the trioctahedral character of the saponite layers formed [64]. The ~3440 cm^{-1} band was assigned to the ν(OH) of physisorbed/interlayer water molecules with the associated bending vibration at 1635 cm^{-1}. The shoulder at about 3220 cm^{-1} was interpreted as the O–H stretching vibrational mode involving hydrogen bonding. The spectra also exhibited lattice vibrations at 1010, 815, 660 and 450 cm^{-1} attributed to, ν(SiO), apical δ(AlO) in AlO_4 units, δ(Mg_3-OH), and δ(Si–O–Mg) bending modes, respectively.

Hydrothermally synthesised (from 125 °C up to 280 °C) saponites were studied by FT-Raman and FTIR spectroscopy and related to naturally occuring saponite by Kloprogge and Frost [34]. FTIR spectra with increasing synthesis temperature provided information about a possible crystallisation scheme from an amorphous starting gel (Figure 6a). A band at 457 cm^{-1} corresponding to the amorphous gel changed, at 280°C, into two distinct bands at 447 cm^{-1} and 465 cm^{-1}, respectively, which was attributed to e_1^2 translational modes of SiO_2 and AlOH of the saponite. Above 150°C, a small band associated with the octahedral sheet in the saponite structure appeared at about 530 cm^{-1} (δ(M_3-OH) perpendicular mode), followed by a band around 750 cm^{-1} (δ(AlMg-OH) deformation mode) above 200°C. At 200˚C, two bands attributed to the a_1^2 SiO_2 and apical Al–O bond of AlO_4 in the tetrahedral sheet were observed at 691 and 837 cm^{-1}, respectively. The most intense SiO_2 band showed a continuous shift from 1043 to 1013 cm^{-1} with increasing synthesis temperature. Two overlapping bands at about 660 and 690 cm^{-1} became visible before the loss of the wide band around 1240 cm^{-1} attributed to amorphous starting gel ν(SiO), suggesting that the octahedral and tetrahedral sheets formed nearly at the same time during crystallisation of saponite. Sharpening of other bands associated with various ν(SiO) modes was not visible until the synthesis temperature reached 200 °C. The corresponding FT-Raman spectra suggested that with increasing temperature, the first internal tetrahedral vibrational mode to become visible was at 683 cm^{-1} (at 150 °C), followed by the band at 360 cm^{-1} (175 °C). Finally, at about 240–280 °C, two bands around 430–465 cm^{-1} became visible (Figure 6b).

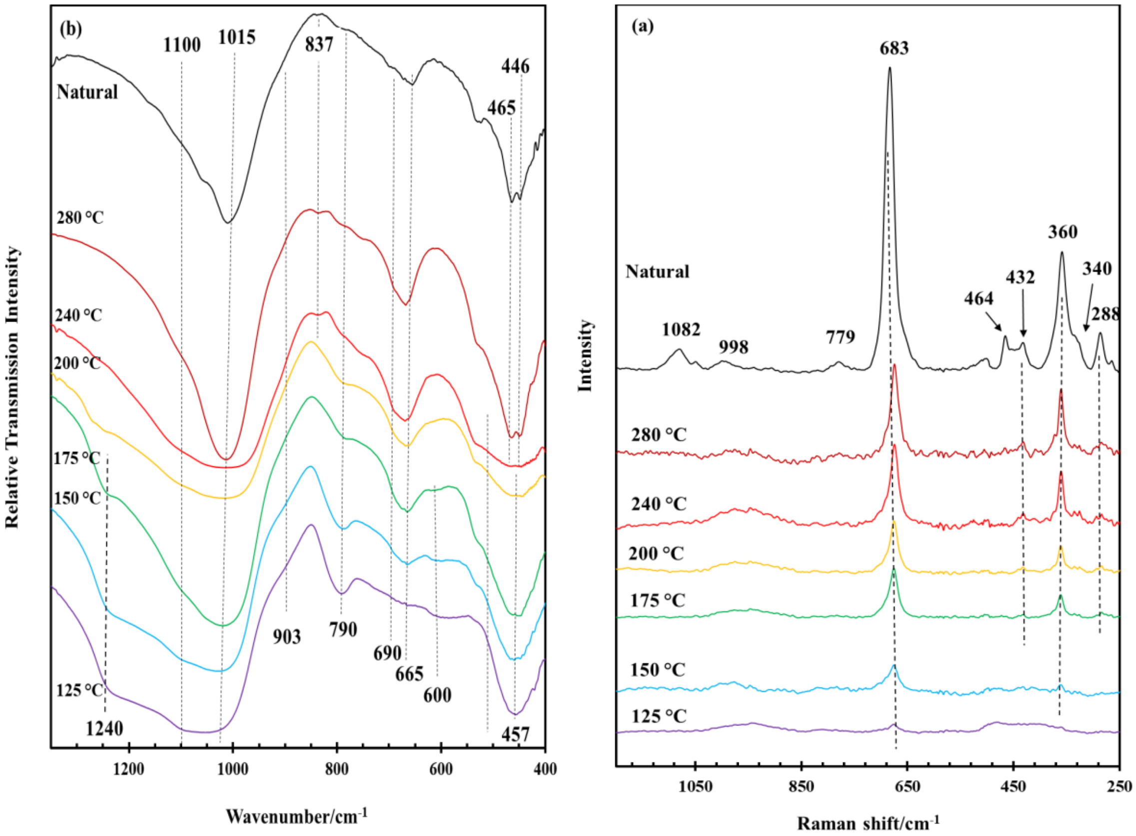

Figure 6 (a) Mid-IR spectra of of synthetic NH_4-saponite synthesized at temperatures between 125 and 280 ˚C in comparison to Milford saponite between 1350 and 400 cm^{-1}; (b) Raman spectra of the same samples in the region between 1200 and 250 cm^{-1} (modified after [34]).

3.3. *Effect of NH_4/Al and H_2O/(Si+Al) ratios during hydrothermal synthesis*

Figure 7 shows the significant similarity in the MIR spectra in the region from 1800 cm^{-1} to 400 cm^{-1} of saponites hydrothermally synthesised from amorphous starting gels with increasing NH_4/Al ratio at 280 ˚C [25,55]. Only minor differences were observed in the band positions and intensities. The bands determined in the MIR spectra of these synthetic saponites are very similar those of natural saponites, even though some Si-O vibrational modes have a very low intensity or absent in the spectra of the synthetic saponites. The band at 1430 cm^{-1} associated with the exchangeable interlayer cation NH_4^+ is similar to the band observed at 1435 cm^{-1} for the synthetic NH_4-mica tobelite [65]. though the band is slightly shifted towards lower wavenumbers possibly as a result of the hydration and higher degree of freedom of NH_4^+ in the interlayer space of saponite. A very small amount of amorphous material was detected in the MIR spectra as low intensity bands at about 1254, 912 (shoulder), 779 and 446 cm^{-1}. Increasing the initial NH_4/Al ratio in the starting amorphous gel had only a small influence on the pH during the synthesis and on the cation exchange capacity (between 33 and 45 meq/100 g) but no distinct influence was observed in the MIR spectra. No intensity increase of the NH_4-band at about 1430 cm^{-1} was detected. The incorporation of only a very small amount of NH_4^+ in the interlayer space of the synthetic saponites was due to the fact that under the hydrothermal synthesis conditions a significant portion of total ammonium will be present in the vapour phase and not in the reaction mix and consequently the ammonium was not included in the saponite structure as the interlayer cation.

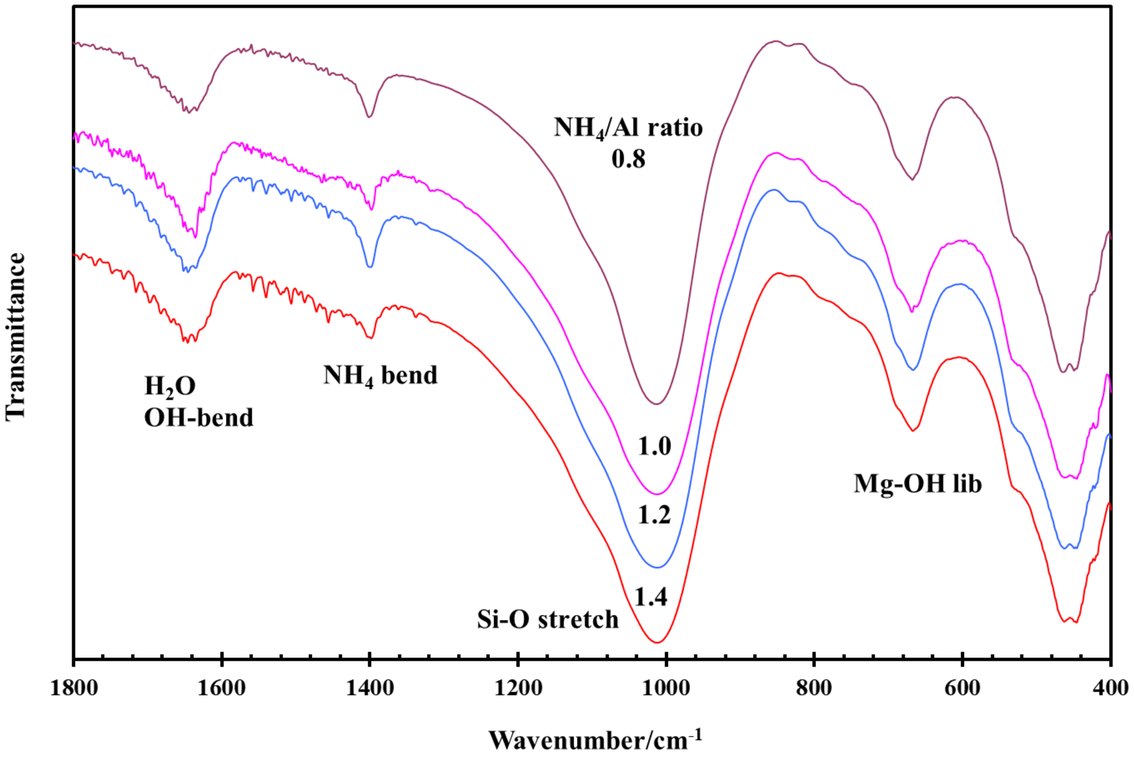

Figure 7. Mid-IR spectra in the region between 1800 and 400 cm^{-1} of NH_4-saponites synthesized with different NH_4/Al ratios at 280 ˚C (modified after [55]).

Figure 8 shows the low wavenumber region of the synthetic NH_4-saponites as a function of the H_2O/(Si+Al) ratio in the amorphous starting gel. The crystalline structure of the saponite was not influenced but the volume of water present in the saponite interlayer space increased from H_2O/(Si +Al) ratio of 10 to 15 and then appeared to remain constant. This indicates that at a H_2O/(Si+Al) ratio of 15 the saponite interlayer space was saturated with water. The water OH-stretching modes at about 3220 and 3430 cm^{-1} likewise showed this. In an earlier publication it was determined that the amount of water present during the hydrothermal synthesis of NH_4-saponite affected the average saponite particle size, saponite crystallinity, and the remaining amount of amorphous material [25]. This is visible in Figure 8 by the increased definition of the different bands in the region from 400 to around 1200 cm^{-1} , which are associated with vibration modes within the saponite layer structure. Very distinct examples are the bands at 740, 779, 836, and 912 cm^{-1}, attributed to Al-OH deformation, amorphous, Al-O apical AlO_4 and amorphous vibrational modes, respectively. The amorphous bands point to a small increase in the amount of amorphous material remaining with increasing water content, which was not detected earlier using XRD and TEM [25]. Moreover, with increasing H_2O/(Si + Al) ratio the amount of NH_4^+ present in the interlayer space appeared to increase marginally, which agrees with the very minor increase in the CEC from 46 to 47 meq/100 g, even though the CEC measurements included all possible exchangeable cations

(Mg^{2+}, Al^{3+} and NH_4^+) and perhaps underestimated the increase in NH_4^+ relative to Mg^{2+} and Al^{3+}. Band deconvolution showed the presence of a minor amount of NH_4^+ by the 3118 cm^{-1} band (Table 2). The other NH_4 -stretching bands at 3300 and 2850 cm^{-1} observed for tobelite [65] were not observed in the NH_4-saponite MIR spectrum. The other bands are vibrational modes attributed to the OH stretching modes of physisorbed and interlayer water, Al-OH, Mg-OH and Si-OH. Here once more, similar to the 1430 cm^{-1} vibration, there was no distinct proof for any influence of the NH_4/Al ratio on the amount of NH_4^+ determined in the saponite interlayer space.

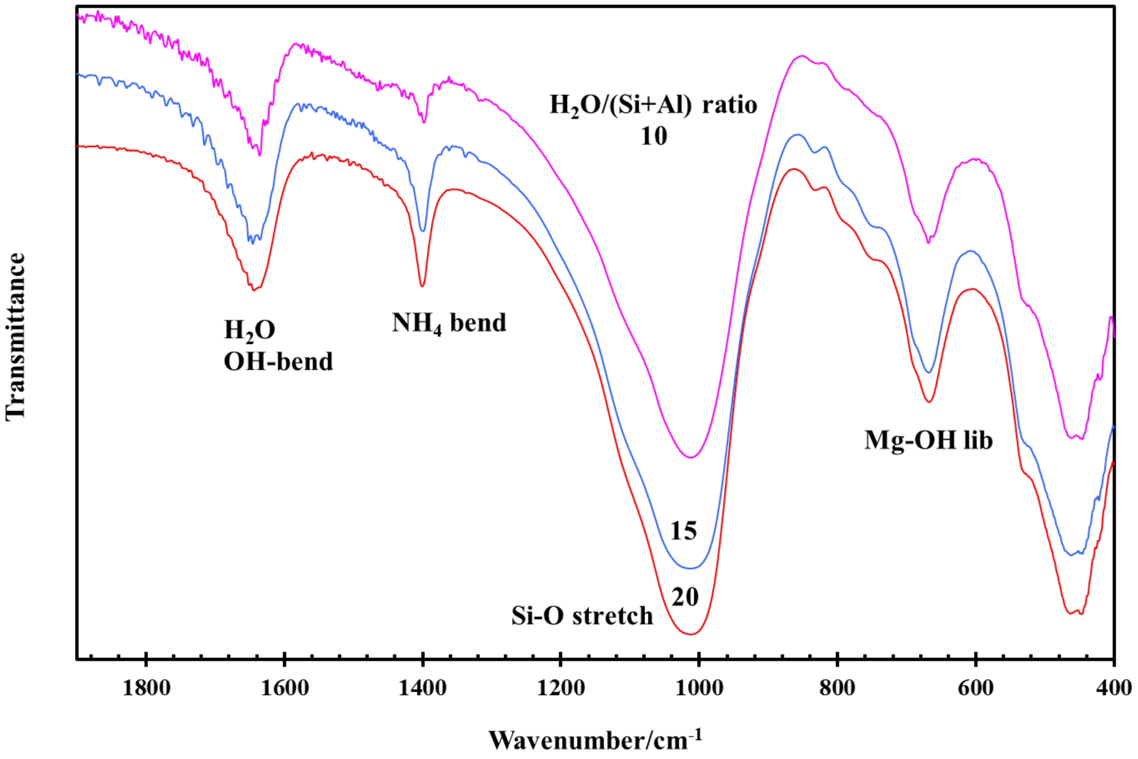

Figure 8. Mid-IR spectra in the region between 1900 and 400 cm^{-1} of NH_4-saponites synthesized with different $H_2O/(Si+Al)$ ratios (modified after [55]).

Table 2 Band positions (cm^{-1}) based on band deconvolution and suggested assignments for the hydroxyl-stretching region of the infrared spectra of synthetic NH_4-saponite in comparison to natural saponite and tobellite

NH_4-saponite	natural saponite	tobellite	assignment [58,65]
		2850	NH_4 stretch
3118		3070	NH_4 stretch
3219	3222		H-O-H stretch
		3300	NH_4 stretch
3432	3420		H-O-H stretch
3590	3625	3630	Al-OH
3662	3680		Mg-OH
3780			Si-OH

3.4. Thermal decomposition of natural and synthetic saponites

The study of thermal changes of saponite (dehydration, dehydroxylation) using in situ spectroscopic techniques has been rather limited. The method of measuring discrete vibrational wavenumbers emitted by thermally excited molecules, called Fourier Transform Infrared Emission Spectroscopy (FTIR ES, or shortly IES) has not been extensively employed to study the thermal behaviour of minerals but in recent years our research group has published extensively on this top, in particular clay minerals [38,50,66-75]. The key benefits of IES can be summarized as: 1) the sample spectra are obtained in situ at increasing temperatures and 2) IES requires no sample treatment other than preparing the sample with submicron particle size as a thin layer on the sample holder. In addition, IES eliminates the problems of heating the samples followed by quenching before measuring an IR spectrum, since IES measures the thermal decomposition process as it is actually occurring.

The IES spectra are similar to the infrared absorption spectra (see section 3.1), though they exhibit a distinct broadening of all bands. Since the first IES spectrum was measured at 200 °C the water OH-bending and OH-stretching modes are less intense and exhibit more noise caused by partial dehydration and the presence of water vapor in the IES cell. Upon heating to 750 °C important differences appear associated with changes in the saponite structure (Figure 9)

.

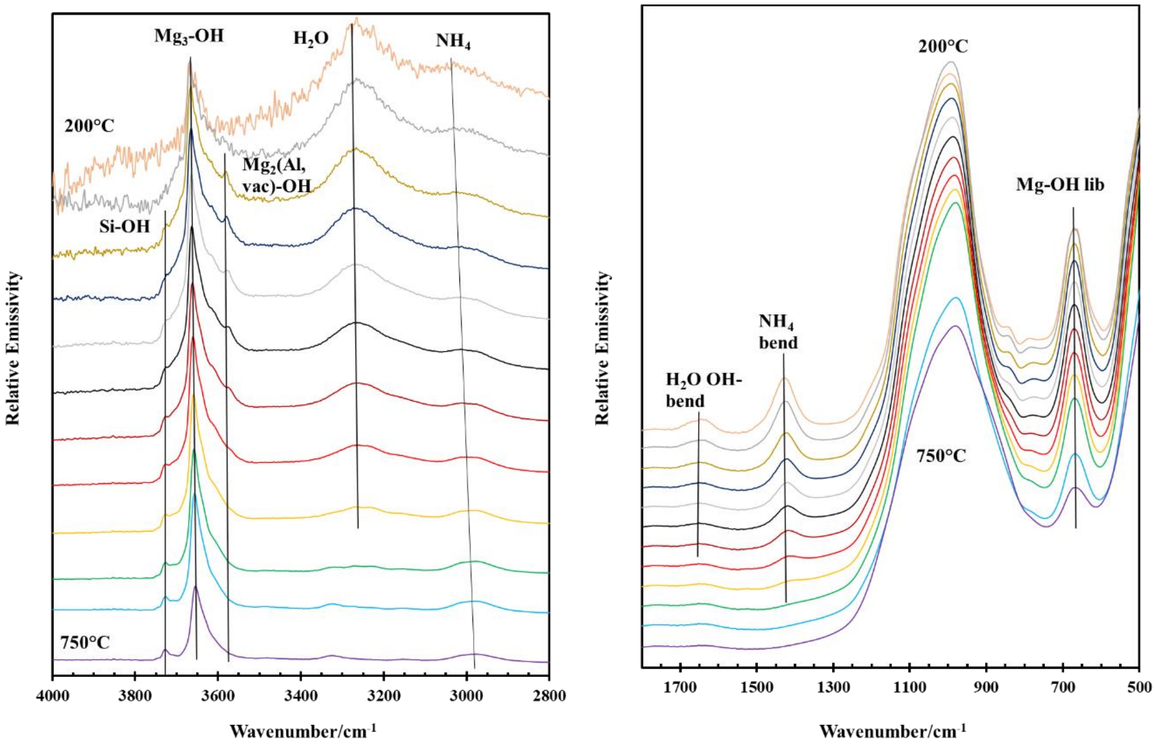

Figure 9. Infrared Emission Spectra of synthetic saponite HTSap1a between 200 and 750 ˚C at 50 ˚C intervals in the regions 4000-2800 cm^{-1} and 1800-500 cm^{-1} (modified after [50]).

The water OH-bending and OH-stretching modes can no longer be distinguised from the background. Upon heating the Si-O stretching modes exhibit a broadening. More important are the changes of the OH-modes, and in the synthetic saponite also the exchangeable cation NH_4-modes, related to the octahedral sheets of the saponites. Thermal analysis of the synthetic saponites provided evidence that dehydroxylation begins around 525 °C,. where it overlaps with the loss of ammonia and the last step of the dehydration (strongly bonded interlayer water), and reaches a maximum between 750 and 860 °C [50]. This agrees well with the dehydroxylation behavior of natural saponites, which typically dehydroxylate above 500 °C and the crystallization of enstatite, $Mg_2Si_2O_6$, around 740 °C [76]. This implies that the dehydroxylation based on the thermal analysis will not be completely finished in the IES. This is rather obvious in Figure y. The 4000-2800 cm^{-1} region exhibits first of all the loss of the interlayer water OH-stretching modes and furthermore an intensity decrease of the OH-band attributed to the Mg_2(Al, vac)-OH mode. On the other hand, the OH-band attributed to the Mg_3-(OH) mode showed a much lower intensity decrease. Comparable observations were made by Frost *et al.* [77], with the dehydroxylation for Milford saponite at approximately 900 °C. This implies that the OH-groups linked to the minor amounts of aluminum or vacancies in the octahedral sheet are not as stable as those linked to only magnesium. Contrary to previous studies on the infrared emission spectroscopy of hectorites and beidellites where silanol, Si-OH, groups were created once the dehydroxylation process started and disappeared after dehydroxylation was finished [73,78], a silanol band is already present at 25 ˚C in the mid-IR spectra of all saponites, which can be observed up to 750 °C in all samples.

The changes in the OH-stretching region are complemented by comparable changes in the region between 1800 and 500 cm^{-1}, where the Mg_2Al-OH translation vibrational mode at about 450 cm^{-1} and the corresponding deformation vibrational mode at about 750 cm^{-1} show an intensity reduction and have disappeared in the 700 °C spectrum. In its place, another band is formed at about 730-740 cm^{-1}. This band can be assigned to the partial restructuring within the saponite's original octahedral sheet and the development of a new Al-O bond after dehydroxylation. This is similar to the formation of a new Al-O band around 722 cm^{-1} observed in dehydroxylated beidellite [73]. Since the dehydroxylation process has not finished at 700-750 °C no different bands pointing to the creation of other Mg-O-Mg, Mg-O-Al or Mg-O-Si bonds can be detected. Only an intensity loss of the Mg_3-OH vibrational modes is visible.

Changes in the IES spectra allow the modelling of the dehydroxylation process of saponite. Generally, dehydroxylation of clay minerals, including smectites such as saponite, entails the release of hydroxyl-groups in the original octahedral sheet through the reaction of two OH groups forming one H_2O molecule and a proton, while at the same time forming a new metal–oxygen bond in the octahedral sheet. This change in the saponite crystal structure is visible in the IES spectra through the decrease and in the end the loss of the bands attributed to the Mg-OH-stretching and Mg-OH-bending modes. Kloprogge *et al.* [73] observed that beidellite dehydroxylation took place through the creation of edge Si-OH groups at temperatures over 400 °C, i.e. the liberated OH^- and H^+ moved from the octahedral sheet to the Si(edge) of the tetrahedral sheet during heating, forming temporarily Si-OH groups before being lost as water vapor. This was reinforced by the disappearance of the Si-OH stretching mode after the dehydroxylation process had finished. The IES spectra of both natural and synthetic saponites do not present support for this model as the Si-OH stretching modes are already present at 25 ˚C in the MIR spectra and did not substantially alter throughout the dehydroxylation up to 750 °C. Nevertheless, it is not impossible that the Si-OH groups act as an active intermediate in the process of dehydroxylation.

4 MAS-NMR of synthetic saponites

Theoretically the synthetic saponite should contain only Al(IV) substituted for Si in the tetrahedral sheet of the saponite structure, while only Mg is present on the octahedral positions. Based on the ^{27}Al MAS-NMR results of the hydrothermally synthesized saponites (Figure 10a) this is clearly not the case as a distinct resonance is observed for Al(VI). This resonance was interpreted as largely being due to substitution of Al in the octahedral sheet for Mg, hence lowering the amount of Al substitution for Si in the tetrahedral sheet and consequently lowering the layer charge. Exchange experiments of ammonium-saponite with $Al(NO_3)_3$ have proven that, although a small increase in Al content and minor change in chemical shift was detected, ^{27}Al MAS-NMR cannot quantitatively differentiate between Al on octahedral sites and on interlayer sites caused by the overlap of the signals. The initially observed 58.3 ppm resonance, which diminished with increasing synthesis temperature, is comparable to the tetrahedral resonance at 57.3 ppm of the starting gel and was attributed to Al present in the amorphous phase (in accordance with the increase of crystallization as shown in Figure 5). Because Al has a quadrupolar nucleus, the Al(IV) : Al(VI) ratio at low magnetic field will be less precise than the Si/Al(IV) ratio based on ^{29}Si MAS-NMR. Fortunately, the error due to spinning sidebands can be excluded in a high magnetic field (11.7 T) and with a high sample spin frequency (14 kHz). The saponites show an increase in Al(IV) to Al(VI) ratio from 1.5 to 3.8 with a hydrothermal synthesis temperature increase from 125 to 280˚C, i.e. with increasing temperature less Al is incorporated in the octahedral sheet moving closer to the ideal saponite composition.

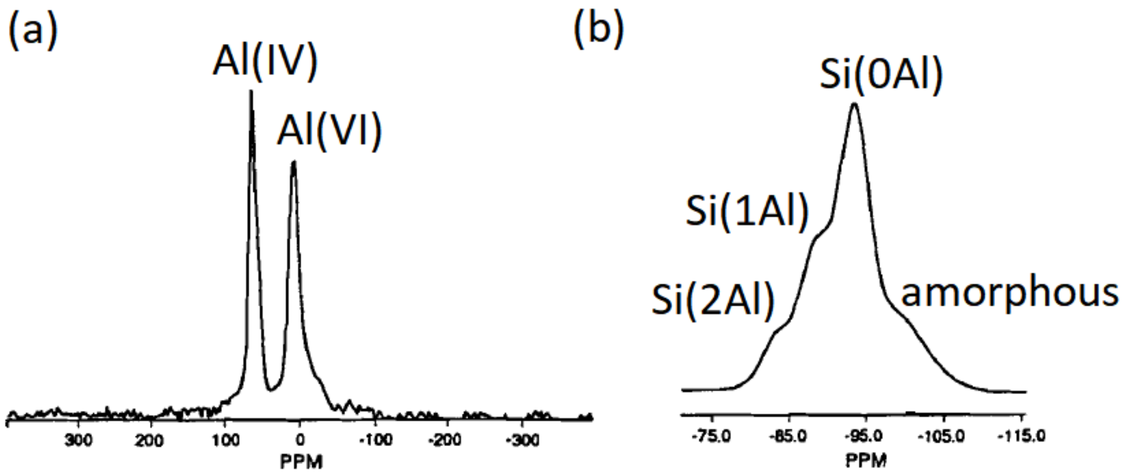

Figure 10 (a). ^{27}A1 MAS-NMR spectrum of synthetic NH$_4$-saponite and, b) ^{29}Si MAS-NMR spectrum of synthetic NH$_4$-saponite (modified from [39]).

^{29}Si MAS-NMR spectra showed three resonances of Si atoms coordinated with one or more next nearest tetrahedral Al atoms in the tetrahedral sheets of the saponite structure. The resonance with the highest intensity was observed at -93.1 + 0.4 ppm assigned to Si(0Al). Furthermore, a shoulder at -88.5 + 0.4 ppm and a small shoulder at -83.2 + 1.2 ppm were distinctly present, and were attributed to Si(1Al) and Si(2Al), respectively [79] (Figure 10b). An additional resonance was initially observed at - 102 ppm, which is due to amorphous material, and diminished with increasing synthesis temperature. The fraction of tetrahedral Al(1Al) linkages and Si(2Al) linkages can be calculated [79] from the resonance intensities. If Loewenstein's avoidance principle is true [80], the fraction of tetrahedral Al(1Al) linkages should be zero. The tetrahedral Al substitution can be calculated directly from the ^{29}Si MAS- NMR spectra using the equation [81]:

$$(\mathrm{Si/Al})^{\mathrm{IV}} = \frac{\sum_{n=0}^{3} I_{Si(nAl)}}{\sum_{n=0}^{3} (\frac{n}{3}) I_{Si(nAl)}} \quad (1)$$

Table 2 Si/Al(IV) ratio and Al(1Al) fraction in the saponite tetrahedral sheets based on ^{29}Si MAS-NMR resonance intensities.

Synthesis temperature (˚C)	Si/Al(IV)	Al(1Al) fraction
125	5.6	0.05
175	5.9	0.04
200	5.1	0.06
240	5.6	0.05
280	5.3	0.05

An average Si/Al(IV) ratio of 5.5 was observed for all saponites, which is very close to the theoretical value of the saponite based on the Si/Al ratio of the starting material (3.4/0.6 = 5.67) (Table 2). The very small fraction of Al(1Al) linkages indicates that the distribution of aluminum in the tetrahedral sheet is close to statistical [82]. Given the results of the ^{27}Al MAS-NMR results this indicates that, despite significant substitution of Al for Mg in the saponite structure, the overall Al for Si substitution remained nearly constant, but the layer charge increased with the increase in synthesis temperature.

The observed ^{29}Si chemical shifts δ are linked to both the overall layer charge and the SiO_4 tetrahedral rotation within the *a*-*b* plane of the saponite layer structure. The rotation of SiO_4 tetrahedra within the tetrahedral sheet is caused by a mismatch in the lateral dimensions between the tetrahedral and octahedral sheets. The *b*-axis length of the tetrahedral sheet is systematically affected by Al(IV) for Si(IV) substitution. The calculation of these parameters from solid state NMR allows one to gain information that cannot be determined from standard powder XRD patterns. The relationship between the chemical shift δ of Si(0Al) and average Si-O-(Si,Al) bond angle θ can be represented as:

$$\delta_{Si(0Al)}(\text{ppm}) = -0619\theta - 18.7 \quad (2)$$

The average deviation a of the Si-O-Si bond angle θ from hexagonal symmetry (θ = 109.47°) allows the determination of the b-axis parameter b_{NMR} using Eq. (3) [83]. An α of 0° signifies an undistorted tetrahedral sheet and may increase to a theoretical maximum of 30°:

$$\cos\alpha = \frac{b_{NMR}}{b_{ideal}} \quad (3)$$

with b_{ideal} being given by Guggenheim [84] as:

$$b(Si_{1-x}Al_x) = 9.15 - 0.74x \quad (4)$$

An alternative method to calculate b_{ideal} was published by Suquet *et al.* [85]:

$$b_{ideal} = 9.174 + 0.079Al(IV) - 007Al(VI) \quad (5)$$

Table 3 ^{29}Si MAS-NMR data and structural parameters, based on the Eqs. 2, 3, 4, and 5 of synthetic NH_4-saponites prepared at increasing hydrothermal temperatures (modified after [39])

Synthesis temperature (°C)	$\theta_{observed}$	$\alpha_{observed}$	b_{ideal} (Å)		b_{NMR} (Å)		b_{XRD} (Å)
			Eq (4)	Eq (5)	Eq (4)	Eq (5)	
125	120.68°	11.21°	9.261	9.212	9.084	9.036	9.175
175	120.03°	10.56°	9.254	9.208	9.097	9.052	9.175
200	121.16°	10.69°	9.270	9.220	9.078	9.029	9.184
240	119.71°	10.24°	9.261	9.217	9.113	9.070	9.174
280	119.39°	9.92°	9.267	9.219	9.128	9.081	9.188

The b_{NMR} values based on the ^{29}Si and ^{27}Al NMR data obtained by Kloprogge *et al.* [39] with both equations were noticeably smaller than the *b*-values observed by XRD (Table 3). Eq. (5) is based on the hypothesis that substitution in the octahedral sheet takes place as one-to-one Mg^{2+} Al^{3+} substitution rather than the usually occurring muscovite substitution of $3Mg^{2+}$ for $2Al^{3+}$ + 1 vacancy, which substitution is followed in Eq. (5). Recalculation of α based on b_{XRD} and b_{ideal} (Eq. 4) produced a minor correction of Eq. (2):

$$\delta_{Si(0Al)}(\text{ppm}) = -0.691\theta - 20.6 \ \pm 0.4 \ (6)$$

while recalculation using b_{ideal} (Eq. 5) produced in a somewhat larger change in Eq. (2):

$$b_{ideal} = -0691\theta - 22.2 \pm 0.5 \ (7)$$

The determined α values were similar to those calculated for other trioctahedral phyllosilicates with average values from 6° to 10° though slightly larger than the values obtained from structural refinements [83]. The slightly smaller correction in Eq. (6) supports the application of the muscovite substitution rather than the one Mg to one Al substitution as used by Suquet *et al.* [85]. This different substitution mechanism has a substantial effect on the charge of the saponite layers and, consequently, on the interlayer composition.

In contrast to the ^{27}Al MAS-NMR results for hydrothermally synthesized saponites, the saponites synthesized using the urea method by Vogels *et al.* [18], though of lower crystallinity showed mainly Al(IV) in its structure with a resonance at about 56 ppm. Only a very weak resonance at 9 ppm was observed for Al(VI). The use of urea in the synthesis clearly had a distinct influence on the coordination of Al during the crystallization limiting the amount of Al(VI) that could substitute for Mg in the octahedral sheets. ^{27}Al and ^{29}Si MAS-NMR experiments were also performed by Vogels *et al.* [18] to determine the influence of the Si/Al ratio on the incorporation of Al^{3+} in the saponite structure. Lowering the concentration of Al^{3+} in the starting material caused a decrease of the Q^3 Si(1Al) resonance, and to a smaller extent of the Q^3 Si(2Al) resonance. The relatively high intensity of the resonance observed at around -86 ppm in saponites synthesized from a gel with a Si/Al ratio of 39.0 is doubtful to be caused by the Q^3 Si(2Al) considering the low concentration of Al^{3+} and the virtually complete disappearance of the Q^3 Si(1Al) resonance. A better interpretation for the resonance at -86 ppm is Q^2 Si(0Al) found at the saponite crystal edges. The synthetic saponites formed with the urea method are composed of extremely small particles (much smaller compared to hydrothermal methods such as the one used by Kloprogge *et al.* [39]) with therefore a high amount of Si^{4+} at the clay edges. The fact that this Q^2 Si resonance in ^{29}Si MAS-NMR spectra of clay minerals is generally not detected may be described to the relatively large particle size of these (natural) samples compared to the urea method synthesized saponite samples.

Vogels *et al.* [86] also studied the substitution of Ga for Al as well as B for Si substitution in the saponite structure. It is expected that Ga^{3+}, like Al^{3+}, can be situated within both tetrahedral, Ga(IV), and octahedral, Ga(VI), coordination sites in the saponite structure. The ^{71}Ga MAS-NMR spectra of Ga^{3+} substituted Mg- and Zn-saponite showed two broad resonances at around 25 and 180–195 ppm, assigned to Ga(VI) and Ga(IV), respectively [87]. For the synthetic Mg-saponites the position of the Ga(IV) resonance was shifted by around +10ppm compared to the Ga(IV) resonance in Zn-saponites. The more positive shift is the result of the higher ditrigonal rotation angle α in the tetrahedral sheets caused by the smaller octahedral sheets in Mg-saponites compared to Zn-saponites. An increase of the rotation angle α has been demonstrated to cause a shift of the resonances of the tetrahedral cations to higher values for related Al^{3+} containing 2:1 phyllosilicates including hydrothermally synthesized saponites [39,81]. Compared to the Al-substituted saponites synthesized with the urea method much more Ga(VI) was formed and substituted in the saponite octahedral sheet.

For most minerals ^{11}B MAS-NMR spectra show a resonance found at about 19 ppm associated with trigonal B^{3+} (BO_3), whereas tetrahedrally coordinated B^{3+} (BO_4) exhibits a resonance at around 2 ppm [52]. Because of the variations in quadrupole coupling constants the BO_3 units are generally observed as broad doublets, while BO_4 resonances are sharp. Substitution of B^{3+} for Si^{4+} in silicate lattices causes a shift to higher field of the BO_4 resonance. The Si/B starting gel for the saponite synthesis only exhibited a sharp resonance around 1.7 ppm, probably due to BO_4 coordinated with SiO_4 tetrahedra. The hydration state did not substantially change the ^{11}B MAS-NMR spectrum of the Si/B gel. The small though noteworthy shift of the BO_4 resonance of the synthetic saponite relative to the gel was assigned to the substitution of B^{3+} for Si^{4+} in the saponite's tetrahedral sheet. Heating to 300 ˚C distinctly proved the transformation of BO_4 units to BO_3. Rehydration of the calcined saponite overnight at 25˚C in a desiccator in the presence of water caused a complete reversal of BO_3 back to BO_4.

5 XPS characterization of natural saponite

Figure 11 gives the survey scan of natural saponite SapCa-2, identifying all the peaks observed. Since XPS is an elemental analysis technique that can independently analyze O the chemical analysis is reported in atom percentages and not in percentages of the oxides as is commonly used in geology. The oxygen content is a function of not only the saponite structure but also of water adsorbed or in the interlayer of the saponite. The XPS results are in good agreement with earlier published chemical analysis, although there are a couple of marked differences. Due to the rather low signal strength of iron (Fe 2p) it is difficult to get a very reliable iron analysis and here no iron was observed though other methods did report a trace of iron. Chlorine (2.2 at%) was observed for SapCa-2, which has not been observed before (Table 4).

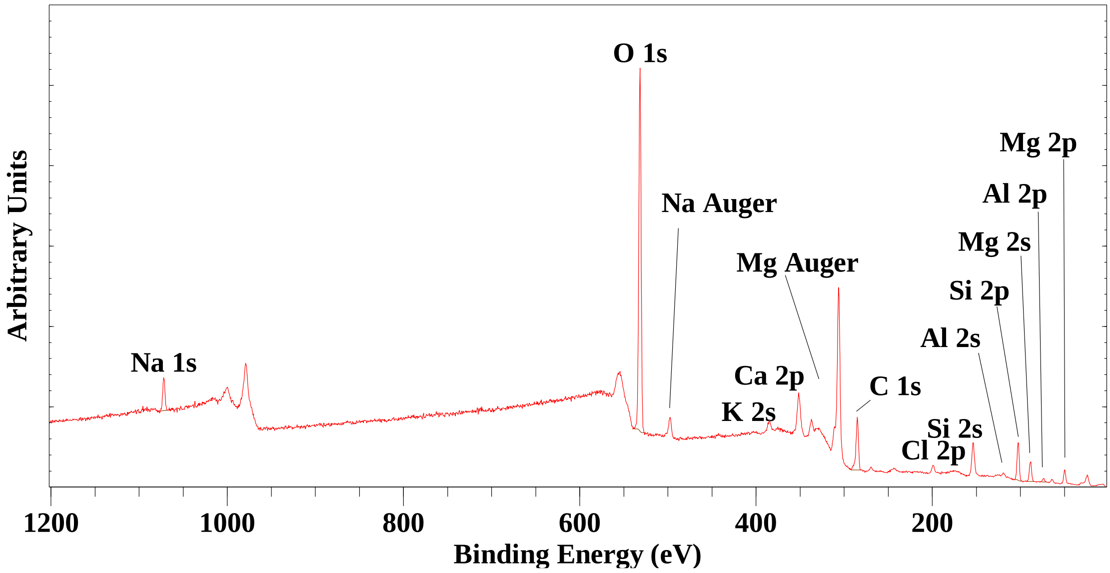

Figure 11. XPS survey scan from 1200 to 0 eV of natural saponite SapCa1.

Table 4 Chemical composition of saponite SapCa-2 (in atom %) based on survey XPS analyses with Si as reference in comparison to data (in atom %) from Datahandbook for Clay Minerals and Other Non-metallic Minerals [88] and Clays and Clay Minerals special issue 49(5) Source Clays (2001)[89]. Oxygen is not included.

Element	XPS	Datahandbook/CCM
Si	22.4	22.39
Al	2.4	2.21
Mg	16.4	15.74
Fe		0.46
Na	3.6	2.02
K	0.5	0.32
Ca	0.5	0.64
Cl	2.2	
Ti		0.02

The Si atoms in saponite are tetrahedrally bonded to O atoms, and form Si–O–Si and Si–O–Al linkages within the tetrahedral sheet and (Al, Fe, Mg)–O–Si linkages between the tetrahedral and octahedral sheet. The binding energy of the Si 2p3/2 is 102.75 eV (line width of about 1.3 eV), which is considerably shifted compared to quartz (α-SiO_2). Kloprogge and Wood [90],[91] and Vantelon *et al.* [92] have shown that the effect of charge and the location of the charge (e.g., tetrahedral substitution of Si^{4+} by Al^{3+} or octahedral substitution of Mg^{2+} by Li^{2+}) triggers an increase in the electronegativity of SiO_4 which causes the decrease in the observed binding energies. In general terms an increase in the Si/Al ratio and the positive shift in binding energy can be correlated with the relative degree of ionicity of the oxide bonds. The Si–O bond is considerably more covalent than the Al–O bond and the relative degree of covalency/ionicity of saponite is altered by the substitution of Al^{3+} for Si^{4+} [93]. Even the position and nature of the exchangeable interlayer cations has a small effect on the electronegativity of the SiO_4 tetrahedra in the tetrahedral sheets. Earlier work in our group on the exchange of Na^+ by an organic surfactant in the interlayer of montmorillonite caused a reduction of the binding energy of about 1 eV together with an increase in the basal spacing from 12.4 to 17.8 Å. This suggests that the binding energy decreases when compensating charges are located further away from the surface in the interlayer space [94]. Other changes in the composition of the octahedral sheet on the Si 2p binding energies are in the order of 0.1 to 0.3 eV, which is not much more than the typical precision of the XPS instrument.

In saponites aluminum can be found both in six-fold coordination in the octahedral sheets and in four-fold coordination in the tetrahedral sheet when substituting for silicon (see previous section on MAS-NMR). According to the Loewenstein avoidance rule no further splitting can be observed as Al atoms are always surrounded by three next-nearest neighboring Si atoms in the tetrahedral sheet or three other metal atoms (e.g. Mg, Fe, Li) in the octahedral sheet preventing the occurrence of Al–O–Al linkages [95,96]. Hence, the Al 2p peak is reasonably symmetric with a relatively narrow width. Curve fitting results in two peak maxima at 73.95 (Al^{IV} 90%) and 74.91 (Al^{VI} 10%) eV with a linewidth of about 1.35 eV. Earlier publications supports this assignment with the binding energy for octahedral Al larger than that of tetrahedral Al [97,98]. Saponite SapCa−2 clearly shows that the majority of the aluminum is present as tetrahedrally coordinated Al and only a fraction is present as octahedrally coordinated Al. These results agree well with other results published for a number of other phyllosilicates [91,92,98,99]. Since the octahedral sheet structure in clay minerals resembles that observed in aluminum hydroxides such as gibbsite, it is not unexpected that the observed binding energy for saponite is indeed similar to those observed for gibbsite and bayerite, (both $Al(OH)_3$) and boehmite (AlOOH) [93,100].

Even though magnesium is one of the major divalent metals in a large number of clay minerals and other phyllosilicates, there are very few papers with Mg 2p and 1s binding energy data for phyllosilicates. Both the Mg 1s and the Mg 2p transitions show in the montmorillonite and vermiculite spectra the presence of two slightly different environments [90]. The ratio of the signals seems to indicate that either 75 or 85% is present in one structural environment and 25 or 15% in the other. Based on the similarity in the positions of the largest peak around 1303 eV in the montmorillonites compared to the saponite this was interpreted as being associated with Mg in octahedral coordination in the clay layers whereas the smaller peak at around 1304 eV is associated with a relatively small amount of interlayer Mg^{2+}. These results contradict earlier results by Vantelon *et al.* [92] who observed only a single Mg 2p peak for saponite.

The O 1s was observed as a strong peak around 532 eV in agreement with other studies of different clay minerals [93,101-103] and micas [104,105]. Notwithstanding the fact that XPS high resolution scans of the O 1 s core spectra are sensitive to the local environment within minerals with octahedral Al structures (see e.g., the difference between O and OH in boehmite [100]) it has not been employed to study clay minerals such as saponite in detail. Because of the ultrahigh vacuum in the XPS instrument no or very little interlayer water can be observed. A split has been found for the smectite group minerals (montmorillonite, beidellite, saponite, hectorite, nontronite) between O and OH with a theoretical ratio of 5:1. For saponite two bands are observed at 531.76 (O 85%) and 533.62 (OH 15%) eV, which is very close to the theoretical value. In reality the O 1s component is much more complex and consists, besides OH, of multiple components associated with what is generally known within silicate structures as bonding and non-bonding oxygen atoms in the layer structure [91,106].

Notwithstanding the relatively low amounts of exchangeable cations in the saponite interlayer spaces compared to the major elements forming the saponite layers and the corresponding lower signal to noise ratio, the exchangeable cations can easily be observed. For Na 1s a single Gaussian band around 1072 eV was detected, which is close to the values reported by Ebina *et al.* [98]. The Ca 2p for exchangeable Ca^{2+} is split in two Gaussian shaped bands Ca 2p1/2 and Ca 2p3/2 bands at 350.7 eV and 347.2 eV. Similarly, K was detected as the K 2p transitions K 2p1/2 around 297.2 eV and K 2p3/2 around 294.3 eV but due to the very low intensity to noise ratio the bands were difficult to accurately fit. Saponite SapCa-2 showed the partial substitution of hydroxyl groups with chlorine. The chlorine was observed as the Cl 2p1/2 and 2p3/2 transitions at 200.58 eV and 198.94 eV.

6. Conclusions

Saponites – i.e. trioctahedral 2:1 smectites with the ideal composition $M_xMg_3Al_xSi_{4-x}O_{10}(OH,F)_2.nH_2O$ (M = exchangeable interlayer cation, e.g. Na^+, NH_4^+, K^+, Ca^{2+}), are easy to synthesize in variable compositions and physicochemical properties, making them attractive for numerous industrial applications including as catalysts, catalysts supports, adsorbent, active ingredient carriers etc. Since the success of the synthesis and the determination of suitable application for the synthetic saponites depends on strong knowledge of the various characterization techniques to ascertain both the saponite structure and properties, this review provided information on the distinguishing characteristics of saponites as determined by a variety of spectroscopic methods. IR and Raman spectroscopy provided information on the positions of the vibrational excitations in saponites and how these are affected by substitutions in the composition and structure of the mineral, as well as during the crystallization and thermal decomposition (dehydration, dehydroxylation, and structural reorganization); MAS-NMR allowed for observation of the Si and Al local environments, in particular Al(IV)/Al(VI) ratio and Si/Al(IV) ratio; and XPS provided information on the chemistry and nature of the local environment of the elements present in the saponite structure and binding energies of these elements of saponites.

Author Contributions: “Conceptualization, CPP and JTK; methodology, JTK; validation, JTK.; formal analysis, JTK; investigation, JTK; resources, JTK; data curation, JTK; writing—original draft preparation, CPP and JTK.;

writing—review and editing, CPP and JTK; visualization, JTK; supervision, JTK. All authors have read and agreed to the published version of the manuscript.

Funding: This research received no external funding

Acknowledgments: The authors acknowledge the facilities, and the scientific and technical assistance, of the Australian Microscopy & Microanalysis Research Facility at the Centre for Microscopy and Microanalysis, The University of Queensland.

Conflicts of Interest: The authors declare no conflict of interest.

References

1. Yang, F.; Sun, S.; Chen, X.; Chang, Y.; Zha, F.; Lei, Z. Mg–Al layered double hydroxides modified clay adsorbents for efficient removal of Pb^{2+}, Cu^{2+} and Ni^{2+} from water. *Appl. Clay Sci.* **2016**, *123*, 134-140.
2. Franco, F.; Benítez-Guerrero, M.; Gonzalez-Triviño, I.; Pérez-Recuerda, R.; Assiego, C.; Cifuentes-Melchor, J.; Pascual-Cosp, J. Low-cost aluminum and iron oxides supported on dioctahedral and trioctahedral smectites: A comparative study of the effectiveness on the heavy metal adsorption from water. *Appl. Clay Sci.* **2016**, *119*, 321-332.
3. Seki, Y.; Ide, Y.; Okada, T.; Ogawa, M. Concentration of 2-phenylphenol by organoclays from aqueous sucrose solution. *Appl. Clay Sci.* **2015**, *109-110*, 64-67.
4. Epelde-Elezcano, N.; Martínez-Martínez, V.; Duque-Redondo, E.; Temiño, I.; Manzano, H.; López-Arbeloa, I. Strategies for modulating the luminescence properties of pyronin Y dye–clay films: an experimental and theoretical study. *Phys. Chem. Chem. Phys.* **2016**, *18*, 8730-8738.
5. Matejdes, M.; Himeno, D.; Suzuki, Y.; Kawamata, J. Controlled formation of pseudoisocyanine J-aggregates in the interlayer space of synthetic saponite. *Appl. Clay Sci.* **2017**, *140*, 119-123.
6. Kumaresan, S.; Rama Pawar, R.; Kevadiya, B.D.; Bajaj, H.C. Synthesis of Saponite Based Nanocomposites to Improve the Controlled Oral Drug Release of Model Drug Quinine Hydrochloride Dihydrate. *Pharmaceut.* **2019**, *12*, 105.
7. Vogels, R.J.M.J.; Kloprogge, J.T.; Geus, J.W. Catalytic activity of synthetic saponite clays: effects of tetrahedral and octahedral composition. *J. Catal.* **2005**, *231*, 443-452.
8. Kawi, S.; Yao, Y.Z. Saponite catalysts with systematically varied Mg/Ni ratio: synthesis, characterization, and catalysis. *Micropor. Mesopor. Mater.* **1999**, *33*, 49-59.
9. Mata, G.; Trujillano, R.; Vicente, M.A.; Belver, C.; Fernandez-Garcia, M.; Korili, S.A.; Gil, A. Chromium-saponite clay catalysts: Preparation, characterization and catalytic performance in propene oxidation. *Appl. Catal., A* **2007**, *327*, 1-12.
10. Ménez, B.; Pisapia, C.; Andreani, M.; Jamme, F.; Vanbellingen, Q.P.; Brunelle, A.; Richard, L.; Dumas, P.; Réfrégiers, M. Abiotic synthesis of amino acids in the recesses of the oceanic lithosphere. *Nature* **2018**, *564*, 59-63.
11. Ponce, C.P.; Kloprogge, J.T. Urea-Assisted Synthesis and Characterization of Saponite with Different Octahedral (Mg, Zn, Ni, Co) and Tetrahedral Metals (Al, Ga, B), a Review. *Life* **2020**, *10*, 168.
12. Nityashree, N.; Price, C.A.H.; Pastor-Perez, L.; Manohara, G.V.; Garcia, S.; Maroto-Valer, M.M.; Reina, T.R. Carbon stabilised saponite supported transition metal-alloy catalysts for chemical CO_2 utilisation via reverse water-gas shift reaction. *Appl. Catal. B: Environmental* **2020**, *261*, 118241.
13. Gebretsadik, F.B.; Cesteros, Y.; Salagre, P.; Gimenez-Manogil, J.; Garcia-Garcia, A.; Bueno-Lopez, A. Potential of Cu-saponite catalysts for soot combustion. *Catal. Sci. Technol.* **2016**, *6*, 507-514.

14. Minz, S.; Gupta, R.; Garg, S. Al–Fe and Al–Ti Pillared Saponite Clay Catalysts: Preparation and Characterization. In Proceedings of Sustainable Engineering, Singapore, 2019; pp. 37-48.
15. Vicente, I.; Salagre, P.; Cesteros, Y. Ni nanoparticles supported on microwave-synthesised saponite for the hydrogenation of styrene oxide. *Appl. Clay Sci.* **2011**, *53*, 212-219.
16. Besselink, R.; Stawski, T.M.; Freeman, H.M.; Hövelmann, J.; Tobler, D.J.; Benning, L.G. Mechanism of Saponite Crystallization from a Rapidly Formed Amorphous Intermediate. *Cryst. Growth Design* **2020**, *20*, 3365-3373.
17. Schumann, D.; Hartman, H.; Eberl, D.D.; Sears, S.K.; Hesse, R.; Vali, H. Formation of replicating saponite from a gel in the presence of oxalate: implications for the formation of clay minerals in carbonaceous chondrites and the origin of life. *Astrobiol.* **2012**, *12*, 549-561.
18. Vogels, R.J.M.J.; Kloprogge, J.T.; Geus, J.W. Synthesis and characterization of saponite clays. *Am. Mineral.* **2005**, *90*, 931-944.
19. Xue, S.; Pinnavaia, T.J. Porous synthetic smectic clay for the reinforcement of epoxy polymers. *Micropor. Mesopor. Mater.* **2008**, *107*, 134-140.
20. Sychev, M.; Prihod'ko, R. Characterization and catalytic activity of non-hydrothermally synthesized saponite-like materials. *Stud. Surf. Sci. Catal.* **1998**, *118*, 967-974.
21. Bisio, C.; Gatti, G.; Boccaleri, E.; Marchese, L.; Superti, G.B.; Pastore, H.O.; Thommes, M. Understanding physico–chemical properties of saponite synthetic clays. *Micropor. Mesopor. Mater.* **2008**, *107*, 90-101.
22. Carniato, F.; Bisio, C.; Gatti, G.; Roncoroni, S.; Recchia, S.; Marchese, L. On the Properties of a Novel V-Containing Saponite Catalyst for Propene Oxidative Dehydrogenation. *Catal. Lett.* **2009**, *131*, 42-48.
23. Higashi, S.; Miki, H.; Komarneni, S. Mn-smectites: Hydrothermal synthesis and characterization. *Appl. Clay Sci.* **2007**, *38*, 104-112.
24. Kloprogge, J.T.; Breukelaar, J.; Geus, J.W.; Jansen, J.B.H. Characterization of Mg-Saponites Synthesized from Gels Containing Amounts of Na^+, K^+, Rb^+, Ca^{2+}, Ba^{2+}, or Ce^{4+} Equivalent to The CEC of the Saponite. *Clays Clay Miner.* **1994**, *42*, 18-22.
25. Kloprogge, J.T.; Breukelaar, J.; Jansen, J.B.H.; Geus, J.W. Development of Ammonium-Saponites from Gels with Variable Ammonium Concentration and Water Content at Low Temperatures. *Clays Clay Miner.* **1993**, *41*, 103-110.
26. Vogels, R.J.M.J.; Breukelaar, J.; Kloprogge, J.T.; Jansen, J.B.H.; Geus, J.W. Hydrothermal Crystallization of Ammonium-Saponite at 200 °C and Autogenous Water Pressure. *Clays Clay Miner.* **1997**, *45*, 1-7.
27. Gebretsadik, F.B.; Mance, D.; Baldus, M.; Salagre, P.; Cesteros, Y. Microwave synthesis of delaminated acid saponites using quaternary ammonium salt or polymer as template. Study of pH influence. *Appl. Clay Sci.* **2015**, *114*, 20-30.
28. Trujillano, R.; Rico, E.; Vicente, M.A.; Herrero, M.; Rives, V. Microwave radiation and mechanical grinding as new ways for preparation of saponite-like materials. *Appl. Clay Sci.* **2010**, *48*, 32-38.
29. Trujillano, R.; Rico, E.; Vicente, M.A.; Rives, V.; Ciuffi, K.J.; Cestari, A.; Gil, A.; Korili, S.A. Rapid microwave-assisted synthesis of saponites and their use as oxidation catalysts. *Appl. Clay Sci.* **2011**, *53*, 326-330.
30. Trujillano, R.; Rico, E.; Vicente, M.A.; Rives, V.; Sobrados, I.; Sanz, J. Saponites containing divalent transition metal cations in octahedral positions - Exploration of synthesis possibilities using microwave radiation and NMR characterization. *Appl. Clay Sci.* **2015**, *115*, 24-29.
31. Vicente, I.; Salagre, P.; Cesteros, Y.; Medina, F.; Sueiras, J.E. Microwave-assisted synthesis of saponite. *Appl. Clay Sci.* **2010**, *48*, 26-31.

32. Kloprogge, J.T.; Komarneni, S.; Amonette, J.E. Synthesis of Smectite Clay Minerals: A Critical Review. *Clays Clay Miner.* **1999**, *47*, 529-554.
33. Kloprogge, J.T.; Jansen, J.B.H.; Schuiling, R.D.; Geus, J.W. The interlayer collapse during dehydration of synthetic Na0.7-beidellite: a sodium-23 solid-state magic-angle spinning NMR study. *Clays Clay Miner.* **1992**, *40*, 561-566.
34. Kloprogge, J.T.; Frost, R.L. The effect of synthesis temperature on the FT-Raman and FT-IR spectra of saponites. *Vibr. Spectrosc.* **2000**, *23*, 119-127.
35. Vogels, R.J.M.J.; Kerkhoffs, M.J.H.V.; Geus, J.W. Non-hydrothermal synthesis, characterization and catalytic properties of saponite clays. *Stud. Surf. Sci. Catal.* **1995**, *91*, 1153-1161.
36. Vogels, R.J.M.J.; Kloprogge, J.T.; Geus, J.W. Homogeneous forced hydrolysis of aluminum through the thermal decomposition of urea. *J. Coll. Interf. Sci.* **2005**, *285*, 86-93.
37. Vogels, R.J.M.J.; Kloprogge, J.T.; Geus, J.W.; Beers, A.W.F. Synthesis and characterization of saponite clays: Part 2. Thermal stability *Am. Mineral.* **2005**, *90*, 945-953.
38. Kloprogge, J.T.; Frost, R.L. Infrared emission spectroscopy of clay minerals. *CMS Workshop Lect.* **2005**, *13*, 99-124.
39. Kloprogge, J.T.; Breukelaar, J.; Wilson, A.E.; Geus, J.W.; Jansen, J.B.H. Solid-state nuclear magnetic resonance spectroscopy on synthetic ammonium /aluminum-saponites. *Clays Clay Miner.* **1994**, *42*, 416-420.
40. Russell, J.D.; Fraser, A. Infrared methods. In *Clay Mineralogy: Spectroscopic and Chemical Determinative Methods*, Wilson, M.J., Ed. Chapman and Hall: London, 1994; pp. 11–67.
41. Pelletier, M.; Michot, L.J.; Barres, O.; Humbert, B.; Petit, S.; Robert, J.-L. Influence of KBr conditioning on the infrared hydroxyl-stretching region of saponites. *Clay Miner.* **1999**, *34*, 439–445.
42. Wang, A.; Jolliff, B.L.; Haskin, L.A. Raman spectroscopic characterization of a highly weathered basalt: igneous mineralogy, alteration products, and a microorganism. *J. Geophys. Res.: Planets* **1999**, *104*, 27067-27077.
43. Wang, A.; Freeman, J.J.; Jolliff, B.L. Understanding the Raman spectral features of phyllosilicates. *J. Raman Spectrosc.* **2015**, *46*, 829–845.
44. Pelletier, M.; Michot, L.J.; Humbert, B.; Barres, O.; d'Espinose De La Caillerie, J.-B.; Robert, J.-L. Influence of layer charge on the hydroxyl stretching of trioctahedral clay minerals: a vibrational study of synthetic Na- and K-saponites. *Am. Mineral.* **2003**, *88*, 1801–1808.
45. Rinnert, E.; Carteret, C.; Humbert, B.; Fragneto-Cusani, G.; Ramsay, J.D.F.; Delville, A.; Robert, J.-L.; Bihannic, I.; Pelletier, M.; Michot, L.J. Hydration of a synthetic clay with tetrahedral charges: a multidisciplinary experimental and numerical study. *J. Phys. Chem. B* **2005**, *109*, 23745–23759.
46. Farmer, V.C.; Russell, J.D. Interlayer complexes in layer silicates. The structure of water in lamellar ionic solutions. *Trans. Faraday Soc.* **1971**, *67*, 2737–2749.
47. Farmer, V.C. The layer silicates. In *The Infrared Spectra of Minerals*, Farmer, V.C., Ed. Mineralogical Society: London, 1974; pp. 331–363.
48. Loh, E. Optical vibrations in sheet silicates. *J. Phys. C* **1973**, *6*, 1091–1104.
49. Arab, M.; Bougeard, D.; Smirnov, K.S. Experimental and computer simulation study of the vibrational spectra of vermiculite. *Phys. Chem. Chem. Phys.* **2002**, *4*, 1957–1963.
50. Kloprogge, J.T.; Frost, R.L. Infrared emission spectroscopic study of the dehydroxylation of some natural and synthetic saponites. *Neues Jahrb. Mineral., Monatsh.* **2001**, 446-463.

51. Kloprogge, J.T. Raman spectroscopy of clay minerals. In *infrared and Raman Spectroscopies of Clay Minerals*, Gates, W.P., Kloprogge, J.T., Madejova, J., Bergaya, F., Eds. Elsevier: Amsterdam, 2017; Vol. 8, pp. 150-199.
52. Kloprogge, J.T.; Hammond, M.; Frost, R.L. Low temperature synthesis and characterisation of pecoraite, a nickel containing phyllosilicate. *Neues Jahrb. Mineral., Monatsh.* **2000**, 193-206.
53. Kloprogge, J.T.; Hammond, M.; Hickey, L.; Frost, R.L. A new low temperature synthesis route of fraipontite $(Zn,Al)_3(Si,Al)_2O_5(OH)_4$. *Mater. Res. Bull.* **2001**, *36*, 1091-1098.
54. Kloprogge, J.T.; Hammond, M.; Hickey, L.; Frost, R.L. Low temperature synthesis of cobalt clays. *J. Mater. Sci. Lett.* **2002**, *21*, 931-933.
55. Kloprogge, J.T.; Hickey, L.; Frost, R.L. Infrared study of some synthetic saponites: Effect of NH_4/Al and H_2O/(Si+Al) ratios during the crystallization. *J. Mater. Sci. Lett.* **1999**, *18*, 1401-1403.
56. Kloprogge, J.T.; Jansen, J.B.H.; Geus, J.W. Characterization of synthetic sodium-beidellite. *Clays Clay Miner.* **1990**, *38*, 409-414.
57. Kloprogge, J.T.; Komarneni, S.; Yanagisawa, K.; Frost, R.L.; Fry, R. Infrared study of some synthetic and natural beidellites. *J. Mater. Sci. Lett.* **1998**, *17*, 1853-1855.
58. van der Marel, H.W.; Beutelspacher, H. *Atlas of Infrared Spectroscopy of Clay Minerals and their Admixtures*; Elsevier: Amsterdam, 1974; pp. 396.
59. Velde, B. Infrared OH-stretch bands in potassic micas, talcs and saponites; influence of electronic configuration and site of charge compensation. *Am. Mineral.* **1983**, *68*, 1169–1173.
60. Borade, R.B.; Clearfield, A. Characterization of acid sites in Beta and ZSM-20 zeolites. *J. Phys. Chem. C* **1992**, *96*, 6729–6737.
61. Baldermann, A.; Dohrmann, R.; Kaufhold, S.; Nickel, C.; Letofsky-Papst, I.; Dietzel, M. The Fe-Mg-saponite solid solution series—a hydrothermal synthesis study. *Clay Miner.* **2014**, *49*, 391–415.
62. Cuadros, J.; Dekov, V.M.; Fiore, S. Crystal-chemistry of the mixed-layer sequence talc-talc-smectite-smectite from submarine hydrothermal vents. *Am. Mineral.* **2008**, *93*, 1338–1348.
63. Dill, H.G.; Dohrmann, R.; Kaufhold, S. Disseminated and faultbound autohydrothermal ferroan saponite in Late Paleozoic andesites of the Saar-Nahe Basin, SW Germany: implications for the economic geology of intermediate (sub)volcanic rocks. *Appl. Clay Sci.* **2011**, *51*, 226–240.
64. Madejová, J. FTIR techniques in clay mineral studies. *Vibr. Spectrosc.* **2003**, *31*, 1–10.
65. Voncken, J.H.L.; Wevers, J.M.A.R.; van der Eerden, A.M.J.; Bos, A.M.J.; Jansen, J.B.H. Hydrothermal synthesis of tobelite, $NH_4Al_2Si_3AlO_{10}(OH)_2$, from various starting materials and implications for its occurrence in nature. *Geol. Mijnbouw* **1987**, *66*, 259–269.
66. Kloprogge, J.T.; Frost, R.L. Infrared emission spectroscopy of Al-pillared beidellite. *Appl. Clay Sci.* **1999**, *15*, 431-445.
67. Kloprogge, J.T.; Frost, R.L. Infrared emission spectroscopic study of some natural and synthetic paragonites. *Appl. Spectrosc.* **1999**, *53*, 1071-1077.
68. Kloprogge, J.T.; Frost, R.L. An infrared emission spectroscopic study of synthetic and natural pyrophyllite. *Neues Jahrb. Mineral., Monatsh.* **1999**, 62-74.
69. Kloprogge, J.T.; Frost, R.L.; Fry, R. Infrared emission study of the thermal transformation mechanism of Al_{13}-pillared clay. *Analyst* **1999**, *124*, 381-384.
70. Kloprogge, J.T.; Frost, R.L.; Hickey, L. Infrared absorption and emission study of synthetic mica-montmorillonite in comparison to rectorite, beidellite and paragonite. *J. Mater. Sci. Lett.* **1999**, *18*, 1921-1923.

71. Kloprogge, J.T.; Frost, R.L.; Kristof, J. Application of infrared emission spectroscopy for the study of the dehydroxylation of synthetic paragonite. *Can. J. Anal. Sci. Spectrosc.* **1999**, *44*, 33-36.
72. Kloprogge, J.T.; Fry, R.; Frost, R.L. An Infrared Emission Spectroscopic Study of the Thermal Transformation Mechanisms in Al_{13}-Pillared Clay Catalysts with and without Tetrahedral Substitutions. *J. Catal.* **1999**, *184*, 157-171.
73. Kloprogge, J.T.; Komarneni, S.; Yanagisawa, K.; Fry, R.; Frost, R.L. Infrared Emission Spectroscopic Study of the Dehydroxylation via Surface Silanol Groups of Synthetic and Natural Beidellite. *J. Coll. Interf. Sci.* **1999**, *212*, 562-569.
74. Kloprogge, J.T.; Frost, R.L. Infrared emission spectroscopy study of the dehydroxylation of 10 Å halloysite from a Neogene cryptokarst of southern Belgium. *Geol. Belg.* **2000**, *2*, 213-220.
75. Kloprogge, J.T.; Hickey, L.; Frost, R.L. Heating stage Raman and infrared emission spectroscopic study of the dehydroxylation of synthetic Mg-hydrotalcite. *Appl. Clay Sci.* **2001**, *18*, 37-49.
76. Newman, A.C.D. *Chemistry of clay and clay minerals*; Longman Scientific & Technical: Harlow, UK, 1987; pp. 480.
77. Frost, R.L.; Collins, B.M.; Finnie, K.; Vassallo, A.J. Infrared emission spectroscopy of clay minerals and their thermal transformations. In Proceedings of Clays, controlling the environment : proceedings of the 10th International Clay Conference, Adelaide, Australia, July 18 to 23, 1993, Adelaide, Australia; pp. 219 - 224.
78. Kloprogge, J.T.; Frost, R.L.; Hickey, L. Infrared emission spectroscopic study of the dehydroxylation of some hectorites. *Thermochim. Acta* **2000**, *345*, 145-156.
79. Lipsicas, M.; Raythatha, R.H.; Pinnavaia, T.J.; Johnson, I.D.; Giese Jr., R.F.; Costanzo, P.M.; Roberts, J.L. Silicon and aluminium site distributions in 2:1 layered silicate clays. *Nature* **1984**, *309*, 604-607.
80. Loewenstein, W. The distribution of aluminum in the tetrahedra of silicates and aluminates. *Am. Mineral.* **1954**, *39*, 92-96.
81. Sanz, J.; Serratosa, J.M. ^{29}Si and ^{27}Al high resolution MAS-NMR spectra of phyllosilicates. *J. Amer. Chem. Soc* **1984**, *106*, 4790-4793.
82. Alma, N. C. M.; Hays, G.R.; Samoson, A.V.; Lippmaa, E.T. Characterization of synthetic dioctahedral clays by solid-state silicon-29 and aluminum-27 nuclear magnetic resonance spectrometry. *Anal. Chem.* **1984**, *56*, 729-733.
83. Weiss, C.A.; Altaner, S.P.; Kirkpatrick, R.J. High resolution ^{29}5i NMR spectroscopy of 2:1 layer silicates: correlation among chemical shift, structural distortions, and chemical variations. *Am. Mineral.* **1987**, *72*, 935-942.
84. Guggenheim, S. The brittle micas. In *Micas*, Bailey, S.W., Ed. Mineralogical Society of America: 1984; Vol. 13, pp. 61-104.
85. Suquet, H.; Malard, C.; Copin, E.; Pezerat, H. Variation du parametre bet de la distance basale d_{001} dans une serie de saponites a charge croissante. I. Etats hydrates. *Clay Miner.* **1981**, *16*, 53-67.
86. Vogels, R.J.M.J.; Kloprogge, J.T.; Geus, J.W. Synthesis and characterisation of boron and gallium substituted saponite clays below 100°C at one atmosphere. *Micropor. Mesopor. Mater.* **2005**, *77*, 159–165.
87. Bradley, S.M.; Howe, R.F.; Kydd, R.A. Correlation between ^{27}Al and ^{71}Ga NMR chemical shifts. *Magn. Reson. Chem.* **1993**, *31*, 883-886.
88. van Olphen, H.; Fripiat, J.J. *Data handbook for Clay Minerals and other Non-Metallic Materials*; Pergamon Press: 1979; pp. 346.

doi:10.20944/preprints202011.0312.v1

89. Kogel, J.E.; Lewis, S.A. Baseline Studies of the Clay Minerals Society Source Clays: Chemical Analysis by Inductively Coupled Plasma-Mass Spectroscopy (ICP-MS). *Clays Clay Miner.* **2001**, *49*, 387-392.
90. Kloprogge, J.T.; Wood, B.J. Baseline studies of the Clay Minerals Society Source Clays by X-Ray Photoelectron Spectroscopy. *Clay Sci.* **2018**, *22*, 85-94.
91. Kloprogge, J.T.; Wood, B.J. *Handbook of Mineral Spectroscopy Volume 1. X-ray Photoelectron Spectra*; Elsevier: Amsterdam, 2020; pp. 505.
92. Vantelon, D.; Belkhou, R.; Bihannic, I.; Michot, L.J.; Montarges-Pelletier, E.; Robert, J.-L. An XPEEM study of structural cation distribution in swelling clays. I. Synthetic trioctahedral smectites. *Phys. Chem. Miner.* **2009**, *36*, 593-602.
93. Barr, T.L.; Seal, S.; He, H.; Klinowski, J. X-ray photoelectron spectroscopic studies of kaolinite and montmorillonite. *Vacuum* **1995**, *46*, 1391-1395.
94. He, H.; Zhou, Q.; Frost, R.L.; Wood, B.J.; Duong, L.V.; Kloprogge, J.T. A X-ray photoelectron spectroscopy study of HDTMAB distribution within organoclays. *Spectrochim. Acta A* **2007**, *66*, 1180-1188.
95. Dove, M.T.; Thayaparam, S.; Heine, V.; Hammonds, K.D. The phenomenon of low Al-Si ordering temperatures in aluminosilicate framework structures. *Am. Mineral.* **1996**, *81*.
96. Palin, E.J.; Dove, M.T.; Redfern, S.A.T.; Bosenick, A.; Sainz-Diaz, C.I.; Warren, M.C. Computational study of tetrahedral Al-Si ordering in muscovite. *Phys. Chem. Miner.* **2001**, *28*, 534-544.
97. Gonzales-Elipe, A.R.; Espinos, J.P.; Munuera, G.; Sanz, J.; Serratosa, J.M. Bonding-state characterization of constituent elements in phyllosilicate minerals by XPS and NMR. *J. Phys. Chem. B* **1988**, *92*, 3471-3476.
98. Ebina, T.; Iwasaki, T.; Chatterjee, A.; Katagiri, M.; Stucky, G.D. Comparative study of XPS and DFT with reference to the distribution of Al in tetrahedral and octahedral sheets of phyllosilicates. *J. Phys. Chem. B* **1997**, *101*, 1125-1129.
99. Kloprogge, J.T. Spectroscopic studies of synthetic and natural beidellites: A review. *Appl. Clay Sci.* **2006**, *31*, 165-179.
100. Kloprogge, J.T.; Duong, L.V.; Wood, B.J.; Frost, R.L. XPS study of the major minerals in bauxite: Gibbsite, bayerite and (pseudo-)boehmite. *J. Coll. Interf. Sci.* **2006**, *296*, 572-576.
101. Mosser, C.; Mosser, A.; Romeo, M.; Petit, S.; Decarreau, A. Natural and synthetic copper phyllosilicates studied by XPS. *Clays Clay Miner.* **1992**, *40*, 593-599.
102. He, H.; Barr, T.L.; Klinowski, J. ESCA and Solid-State NMR studies of allophane. *Clay Miner.* **1995**, *30*, 201-209.
103. Johns, W.D.; Gier, S. X-ray photoelectron spectroscopic study of layer-charge magnitude in micas and illite-smectite clays. *Clay Miner.* **2001**, *36*, 355-367.
104. Bhattacharyya, K.G. XPS study of mica surfaces. *J. Electron Spectrosc. Rel. Phenom.* **1993**, *63*, 289-306.
105. Liu, Z.H.; Brown, N.M.D. XPS characterization of mica surfaces processed using a radio-frequency (rf) argon plasma. *J. Phys. D: Appl. Phys.* **1998**, *31*, 1771-1781.
106. Nessbitt, H.W.; Bancroft, G.M. High Resolution Core- and Valence-Level XPS Studies of the Properties (Structural, Chemical and Bonding) of Silicate Minerals and Glasses. In *Spectroscopic Methods in Mineralogy and Materials Sciences*, Henderson, G.S., Neuville, D.R., Downs, R.T., Eds. Mineralogical Society of America: Chantilly, 2014; Vol. 78, pp. 271-329.